U.S. DEPARTMENT OF COMMERCE
National Technical Information Service
PB-298 073

Aerosol Measurements in the Submicron Size Range Studies with an Aerosol Centrifuge, a New Diffusion Battery, a Low Pressure Impactor and an Advanced Condensation Nuclei Counter

Vienna Univ. (Austria). Inst. for Experimental Physics

Prepared for

Environmental Sciences Research Lab., Research Triangle Park, NC

Mar 79

United States
Environmental Protection
Agency

Environmental Sciences Research
Laboratory
Research Triangle Park NC 27711

EPA-600/2-79-105
May 1979

Research and Development

PB 298073

EPA

Aerosol Measurements in the Submicron Size Range

Studies With an Aerosol Centrifuge, a New Diffusion Battery, a Low Pressure Impactor and an Advanced Condensation Nuclei Counter

REPRODUCED BY
NATIONAL TECHNICAL
INFORMATION SERVICE
U. S. DEPARTMENT OF COMMERCE
SPRINGFIELD, VA. 22161

RESEARCH REPORTING SERIES

Research reports of the Office of Research and Development, U S Environmental Protection Agency, have been grouped into nine series. These nine broad categories were established to facilitate further development and application of environmental technology. Elimination of traditional grouping was consciously planned to foster technology transfer and a maximum interface in related fields. The nine series are:

1. Environmental Health Effects Research
2. Environmental Protection Technology
3. Ecological Research
4. Environmental Monitoring
5. Socioeconomic Environmental Studies
6. Scientific and Technical Assessment Reports (STAR)
7. Interagency Energy-Environment Research and Development
8. "Special" Reports
9. Miscellaneous Reports

This report has been assigned to the ENVIRONMENTAL PROTECTION TECHNOLOGY series. This series describes research performed to develop and demonstrate instrumentation, equipment, and methodology to repair or prevent environmental degradation from point and non-point sources of pollution. This work provides the new or improved technology required for the control and treatment of pollution sources to meet environmental quality standards.

This document is available to the public through the National Technical Information Service, Springfield, Virginia 22161.

TECHNICAL REPORT DATA
(Please read Instructions on the reverse before completing)

1. REPORT NO. EPA-600/2-79-105	2.
3. RECIPIENT'S ACCESSION NO. PB298073	
4. TITLE AND SUBTITLE AEROSOL MEASUREMENTS IN THE SUBMICRON SIZE RANGE Studies with an Aerosol Centrifuge, a New Diffusion Battery, a Low Pressure Impactor and an Advanced Condensation Nuclei Counter	5. REPORT DATE May 1979 6. PERFORMING ORGANIZATION CODE
7. AUTHOR(S) Othmar Preining and Axel Berner	8. PERFORMING ORGANIZATION REPORT NO.
9. PERFORMING ORGANIZATION NAME AND ADDRESS Institute for Experimental Physics The University of Vienna A-1090 Wien, Strudlhofgasse 4 Austria	10. PROGRAM ELEMENT NO. 1AD712 BC-16 (FY-78) 11. CONTRACT/GRANT NO. 801983
12. SPONSORING AGENCY NAME AND ADDRESS Environmental Sciences Research Laboratory--RTP, NC Office of Research and Development U. S. Environmental Protection Agency Research Triangle Park, N.C. 27711	13. TYPE OF REPORT AND PERIOD COVERED Final 1973-1978 14. SPONSORING AGENCY CODE EPA/600/09
15. SUPPLEMENTARY NOTES	

16. ABSTRACT

The report summarizes the investigations of four aerosol classifiers which cover finite, but overlapping ranges of the aerosol particle size spectrum. The first part is concerned with a cylindrical aerosol centrifuge, which measures aerodynamic equivalent diameters precisely. This instrument has been used as a reference instrument in diffusion battery experiments reported in the second part. The diffusion battery has been investigated for fairly large particle sizes (0.3 μm to 0.5 μm) to determine the influence of sedimentation, interception and impaction on the transmission of the diffusion battery. These experiments have been performed with highly monodispersed NaCl aerosols. In the third part a five stage low pressure impactor is described, which covers the size range from 0.1 μm to 25 μm diameter. It has been developed specifically for the determination of the deposited particulate mass. First data on mass-size distributions of atmospheric aerosols are reported. The final chapter summarizes the development of a special condensation nuclei counter which measures number-size distributions in the size range from 0.002 μm to 0.1 μm KELVIN-equivalent diameter. The applicability to urban atmospheric aerosols is demonstrated.

17. KEY WORDS AND DOCUMENT ANALYSIS

a. DESCRIPTORS	b. IDENTIFIERS/OPEN ENDED TERMS	c. COSATI Field/Group
Air pollution		13B
*Aerosols		07D
*Particle size		14B
*Centrifuges		13H
Diffusion		11C
Size separation		
Condensation nuclei		
Counters		

18. DISTRIBUTION STATEMENT RELEASE TO PUBLIC	19. SECURITY CLASS *(This Report)* CLASSIFIED 20. SECURITY CLASS *(This page)* CLASSIFIED	21. NO. OF PAGES 109 22. PRICE A F06/MF A01

EPA Form 2220-1 (Rev. 4-77) PREVIOUS EDITION IS OBSOLETE

EPA-600/2-79-105
May 1979

AEROSOL MEASUREMENTS IN THE SUBMICRON SIZE RANGE

Studies with an Aerosol Centrifuge, a New Diffusion Battery, a Low Pressure Impactor and an Advanced Condensation Nuclei Counter

by

Othmar Preining and Axel Berner
Institute for Experimental Physics
University of Vienna
Austria

Research Grant No. 801983

Project Officer

Jack Wagman
Director, Emissions Measurement and Characterization Division
Environmental Sciences Research Laboratory
Research Triangle Park, North Carolina 27711

ENVIRONMENTAL SCIENCES RESEARCH LABORATORY
OFFICE OF RESEARCH AND DEVELOPMENT
U. S. ENVIRONMENTAL PROTECTION AGENCY
RESEARCH TRIANGLE PARK, NORTH CAROLINA 27711

DISCLAIMER

This report has been reviewed by the Environmental Sciences Research Laboratory, U. S. Environmental Protection Agency, and approved for publication. Approval does not signify that the contents necessarily reflect the views and policies of the U. S. Environmental Protection Agency, nor does mention of trade names or commercial products constitute endorsement or recommendation for use.

PREFACE

Polluting the atmosphere is one of man's most traditional ways to dispose of unwanted products from cultural and industrial activities. But today's large scale pollution forces society to regard its economical activities with careful respect of man's and other beings' health. Related research programs are still a demand in order to meet the needs for sufficient information to make the necessary political decisions weighing calculable risks versus economic benefits.

The Institut für Experimentalphysik, formerly I. Physikalisches Institut of the University of Vienna has been and still is involved in a number of research programs on the atmospheric environment, particularly it has a long historic record in aerosol research dating back as far as the first decade of this century. Present research is mainly concerned with visibility and respective aerosol photometers, cascade impactors, condensation nuclei counters, their fundamentals and their applications to atmospheric aerosols.

Prof. Dr. P. Weinzierl
Head
Institut für Experimentalphysik
University of Vienna

BACKGROUND

The longer research continues the more the importance of aerosols becomes evident for all aspects of air pollution. The problems of recent interest are related to industrial and civic hygiene in local environments as well as to the global pollution of the earth's atmosphere. At all levels the aerosol problems are of great, and mostly not completely understood complexity. Hence the analysis of aerosols requires profound knowledge of their physical and chemical properties.

The dynamics of aerosols, i.e. the development of the physical and chemical properties in time, is a focus of todays' interest, and refined measuring techniques are required in order to produce basic data such as aerosol size distributions and the chemical composition of the different particle sizes. Difficulties arise, because aerosol classifiers are generally not able to cover the whole size range of interest. Hence different instruments are to be combined into classifier systems in order to yield complete information. New problems arise. The system components evaluate aerosol properties within limits only, and moreover they may distort the information - problems which can be recognized and overcome only by comparisons of different system.

In the past, this system approach led to the development of the University of Minnesota Aerosol Classifying System, which led to profound insights into the structure of aerosol size distributions. But this system has its limitations, too , and it is unsuitable for collecting chemically analyzable samples. New techniques are required in order to meet such needs.

ABSTRACT

The report summarizes the investigations of four aerosol classifiers which cover finite, but overlapping ranges of the aerosol particle size spectrum.

The first part is concerned with a cylindrical aerosol centrifuge, which measures aerodynamic equivalent diameters precisely. This instrument has been used as a reference instrument in diffusion battery experiments reported in the second part. The diffusion battery has been investigated for fairly large particle sizes (0.3 μm to 0.5 μm) to determine the influence of sedimentation, interception and impaction on the transmission of the diffusion battery. These experiments have been performed with highly monodispersed NaCl aerosols.

In the third part a five stage low pressure impactor is described, which covers the size range from 0.1 μm to 25 μm diameter. It has been developed specifically for the determination of the deposited particulate mass. First data on mass-size distributions of atmospheric aerosols are reported. The final chapter summarizes the development of a special condensation nuclei counter which measures number-size distributions in the size range from 0.002 μm to 0.1 μm KELVIN-equivalent diameter. The applicability to urban atmospheric aerosols is demonstrated.

CONTENTS

Preface iii
Background iv
Abstract v
Figures ix
Tables xiii
Acknowledgement xiv

Conclusions 1
Recommendations 3

The ROSL Aerosolspectrometer
- Introduction 4
- Rotors of the ROSL Spectrometer 6
- Particle Size Analysis 9
- Operational Features of the ROSL Spectrometer 15
- Discussion 26

The Diffusion Battery
- Introduction 28
- The NaCl Generator 31
- The NaCl Aerosols 36
- The Diffusion Battery 45
- Deposition Mechanisms in a Diffusion Battery 48
- Results and Discussion 54

Preceding page blank

The Five Stage Low Pressure Impactor

Introduction 6o

Particle Size Analysis 63

The Aerodynamic Equivalent Size 66

Deposits in the Impactor Stages 68

Note on Back Up Filters 74

The Condensation Nuclei Counter

Introduction 77

The Expansion Cloud Chamber and its Data Acquisition System 77

The Analysis of the Recorded Data 81

Results on Atmospheric Aerosols 84

References 87

FIGURES

1 Cross section of rotor I. B, base plate; MC, measuring chamber; CC, cleaning chamber; S, aerosol slit; H, ports to the cleaning chamber; K, shaft. 5

2 Cross section of rotor II. B, base plate; MC, measuring chamber; S, aerosol slit; K, shaft; AFLO, aerosol flow limiting orifice; TFLO, total flow limiting orifice. 7

3 Head of rotor I with gasket. N,nylong spring disc; S,teflon sheet 8

4 Latex aerosol deposits on collection foil. S, projection of the slit. 1), single spheres, 2) to 5), aggregates of 2,3,4,5 spheres 8

5 Number size distribution of latex aerosol. 1), single spheres; 2) to 5), aggregates of two to five spheres. 11

6 The reduced deposition length and its relationship to the equivalent particle size, calculated from DOW quotations. Bars indicate the average and the range of the experimental data, the solid line represents the theoretical expectation 17

7 Variance of number size distributions of single latex particles and its relationship to the cross section of the AFLO orifice.... 18

8 Number size distributions of single latex spheres at different AFLO cross sections. 2o

9 Calibration curves of the aerosol centrifuge. 22

1o Calibration curves of the aerosol centrifuge 22

11 Ambivalent deposition lengths..... 23

12 Range of speed fluctuations for the system rotor II/regulated power supply..... 23

13 Number size distributions of single latex particles for cold and warmed rotor I. 25

13a Calibration curves for rotor II. 27

14 Furnace for the generation of monodispersed NaCl aerosols..... 29

15 Cross section of the aerosol generator 3o

16 Calibration curves for the gas temperatures in the center tube... 33

17 Gas temperatures along the axis of the center tube 34

18 Gas temperatures along the axis of the center tube,æro flow rate.. 35

19 The sizes of the monodispersed NaCl aerosols in dependence of the temperatures at zone I and zone II..... 37

2o Number size distribution of heavily coagulated NaCl aerosols..... 39

21 Number size distribution of weakly coagulated NaCl aerosols..... 4o

22 Number size distribution of diluted NaCl aerosols 42

23 Number size distribution of diluted NaCl aerosols 43

24 Comparison of electron microscopical diameters of NaCl particles to their deposition lengths in the centrifuge..... 44

25 Cross section of the diffusion battery..... 46

26 Tubing diagram of the diffusion battery..... 47

27 Theoretical impaction and interception efficiency of CHS plates .. 53

28 Experimental transmission data compared to theoretical expectations..... 57

29 Cross section of the fice stage low pressure impactor..... 61

3o Wall losses in the five stage impactor..... 7o

31 Variations of deposited mass among the spots 72

32 Mass size distribution of a vaseline-dye-aerosol 73

33 Mass size distribution of an urban aerosol at Vienna..... 73

34 Threehourly variations of urban aerosols at Vienna 75

35 Diagram of the data acquisition system of the condensation nuclei counter 78

36 Aerosol and gas flow diagram of the condensation nuclei counter .. 8o

37 Scattered light intensity of the growing aerosol. 82

38 Scattered light intensity calculated from the MIE theory..... 83

39 Cumulative number size distribution of KELVIN euqivalent diameter 85

4o. Differential number size distribution of KELVIN equivalent diameter for an urban atmospheric aerosol at Vienna..... 86

TABLES

Number		page
1	Analysis of Latex particle deposits	16
2	Experimental and theoretical transmissions of the diffusion battery	55
3	Deviations of theoretical Transmissions from Experimental values	58
4	Data of the impactor stages	62

ACKNOWLEDGEMENTS

The research program has been sponsored by the Environmental Protection Agency of the United States of America and by several Austrian Governmental and Municipial Organizations including the Bundesministerium für Wissenschaft und Forschung, The Fonds zur Förderung der wissenschaftlichen Forschung and the Hochschuljubiläumsstiftung der Stadt Wien. The support by these organizations is gratefully acknowledged.

The authors wish to express their personal gratitude to the staff of the Institute. Dr. Gerhard Kasper conducted successfully the research on the diffusion battery, Dr. Paul Wagner, assisted by Mr. Franz Pohl, is responsible for the study of the condensation nuclei counter. Mr. Christian Lürzer performed the measurements of the urban mass size distributions. The authors are greatly indepted to Mrs. Hannelore Kranner who performed the work of typing and assembling the report with extraordinary patience.

CONCLUSIONS

The results of the work reported here demonstrate:

1) The aerosol centrifuge is an instrument for measuring aerodynamic diameters precisely and independent of external calibrations such as calibrations by latex particles. So far the instrument has been investigated for particle sizes from o,2 µm to 3,o µm diameter, but there are indications that the instrument is capable to classify particles as small as o,o5 µm, at suitable operation conditions.

2) The diffusion battery can be operated up to sizes of o,5 µm diameter, if great care is taken in calibrating the instrument. For such particles sizes impaction becomes an essential deposition mechanism.

3) Highly monodispersed NaCl aerosols with spherical particles of bulk density can be produced by a generator of the SINCLAIR-LA MER type. The aerosol properties are controlled by the cooling rate of the condensing vapours.

4) Cascade impactors have been designed as to permit the direct and accurate measurement of mass size distributions of atmospheric aerosols. The first impactor under investigation has a measuring range from o,1 µm to 25 µm, permitting the gravimetric evaluation of the accumulation mode of atmospheric aerosols. There are indications that an impactor can be designed for the collection sizes as small as o,o5 µm diameter or less.

5) The condensation nuclei counter technique can be used to determine number size distributions of atmospheric aerosols in the size range from o,oo2 µm to o,1 µm of KELVIN equivalent diameter.

6) The combination of a cascade impactor and a condensation nuclei counter of the kind described here would constitute a system for the evaluation of size distributions in the range from o,oo2 µm to 25 µm diameter, with a sufficient overlap at sizes around o,1 µm diameter. Moreover, the data of the system components would be fairly independent of each other, because the nucleation mode would represent almost completely the total particle concentration by number, but does not contribute considerably to the total particle concentration by mass.

RECOMMENDATIONS

Since an aerosol sizing system of a cascade impactor and a condensation nuclei counter as described in this report permits to evaluate the size distribution of atmospheric aerosols in the same size range as the University of Minnesota Aerosol Sizing System, a direct comparison of both systems could provide so far unobtained insights in the structure of atmospheric aerosols as well as in the operation characteristics of the classifier systems.

THE ROSL AEROSOL SPECTROMETER

Introduction

Aerosol centrifuges are well known instruments for the classification of aerosols. Since their introduction by SAWYER and WALTON (1) in 195o they underwentlarge improvements which culminated in the development of several highly resolving spectrometers. The work of GÖTZ et al.(2,3,4), KEITH and DERRICK (5), KAST (6), STÖBER and coworkers (7), (8), (9), (1o), (11), (12), HAUCK and SCHEDLING (13), HOCHRAINER (14), (15), BERNER and REICHELT (16), BURSON et al (17), and MATTESON et al (18) may be quoted here.

The main idea of these instruments is the separation of the aerosol particles from a steady, laminar flow by means of the centrifugal force. For this purpose the aerosol is introduced into a rotating chamber. Under the influence of the force the particles move to the outer wall where they are deposited on a removable foil. Classification occurs because the particle velocities produced by the centrifugal force depend on the particle sizes: the larger the particles are, the faster they drift to the wall. Complete classification is achieved when the aerosol is introduced into the chamber by a narrow slit which superimposes the aerosol on a layer of particle free gas. For a thin aerosol layer the particles fall to the outer wall from almost identical positions, and their deposit location with respect to the entrance slit, i.e. the deposition length, is a direct measure of their size because a given location corresponds to only one particle size.

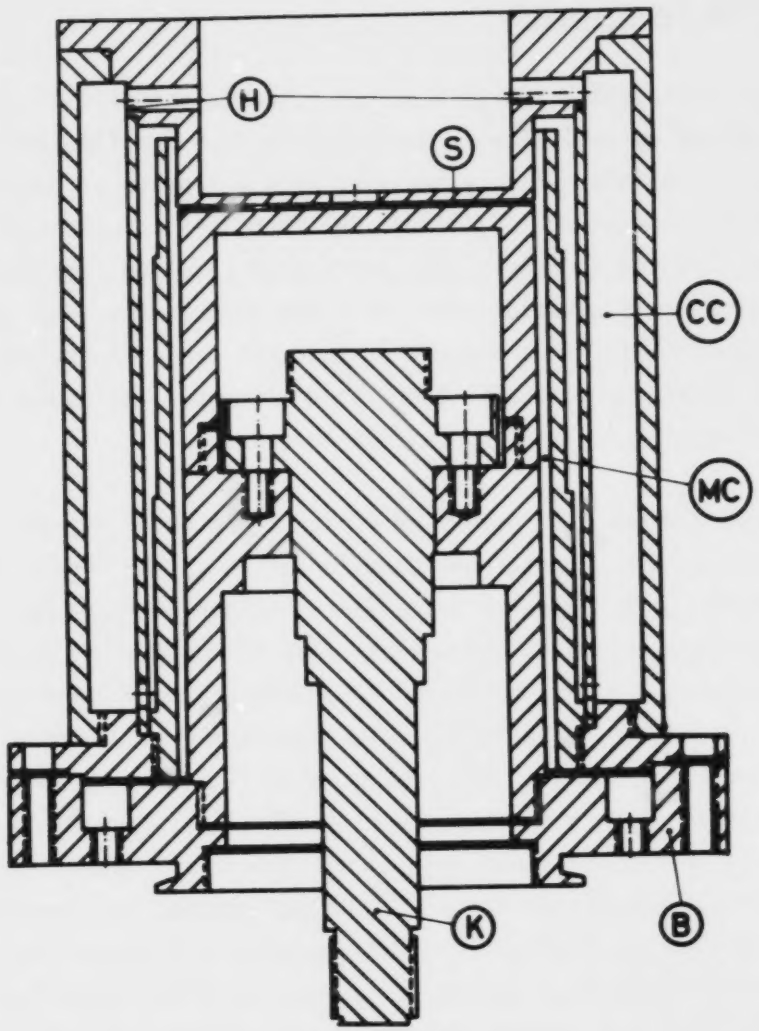

Fig.1: Cross section of rotor I. B,base plate; MC, measuring chamber; CC, cleaning chamber ; S, aerosol slit ; H, ports to the cleaning chamber; K, shaft.

Rotors of the ROSL spectrometer

An adequate slit system has to meet one essential condition: the superposition of the aerosol flow on the particle free gas flow should be as undisturbed as possible. This is achieved when all parts of the slit participate fully in rotation (19), (2o). The technical solutions of this problem are very limited in number. The particular solution realized in the ROSL spectrometer is a radial slit, or a cut through the inner parts of the rotor (see fig. 1). This concept of the slit leads almost forcibly to a concentric arrangement of all other rotor elements. The choice has been given to concentric cylinders, but not to cones.

In operation the rotor is driven by a high speed motor via the shaft K and the flow is maintained by the selfpumping action of the rotor. The aerosol flow enters the slit S by an orifice in the center of rotation. This socalled AFLO orifice restricts the aerosol flow to the desired magnitude. Partially particle free gas is produced by the rotor itself. Some aerosol is passed through several holes, H, into a cleaning chamber, CC, where large particles are removed from the gas. The remaining particles are usually too small as to be detected by light microscopy. Particles of this background aerosol will be deposited on the foil, but they do not appear optically. This cleaning procedure bears some advantage. At first, the gas composition remains unchanged and therefore the superposition of the aerosol flow and the particle free flow is not influenced by density gradients. Secondly, external filtering devices are unnecessary as long as the remaining particles do not interfere with the observations. The particle free flow enters the measuring chamber, MC, through a port in the top of the rotor. Another rotor of slightly different design is shown in fig. 2. In this case the particle free gas is not produced in a cleaning chamber, but it is drawn from the flow boundary layer at the outside of the rotor. The gas is particle free to the same degree as described above. Size classification is bound to laminar flow in the measuring chamber, therefore the total amount of flow has to be limited. Adequate restriction is achieved by a set of six orifices, i.e. the TFLO or total flow limiting orifices, in the bottom of each rotor. In order to change the collection foils the rotors are disassembled by lifting the outer parts comprising the

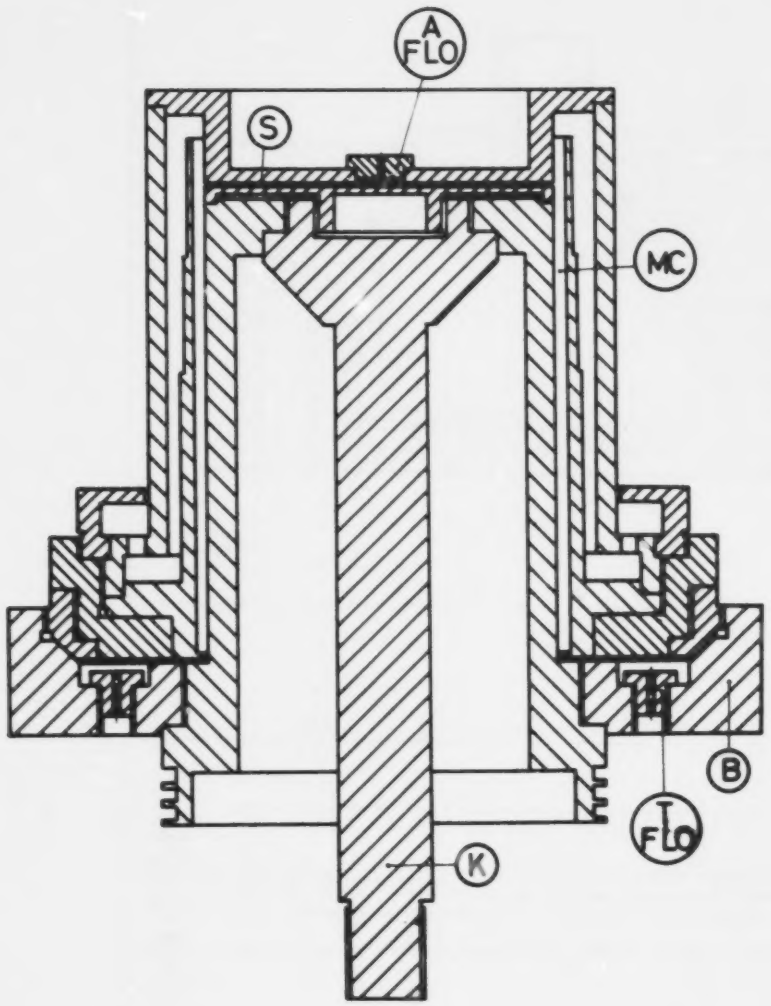

Fig.2 : Cross section of rotor II. B, base plate; MC, measuring chamber; S, aerosol slit; K,shaft; AFLO, aerosol flow limiting orifice; TFLO, total flow limiting orifice.

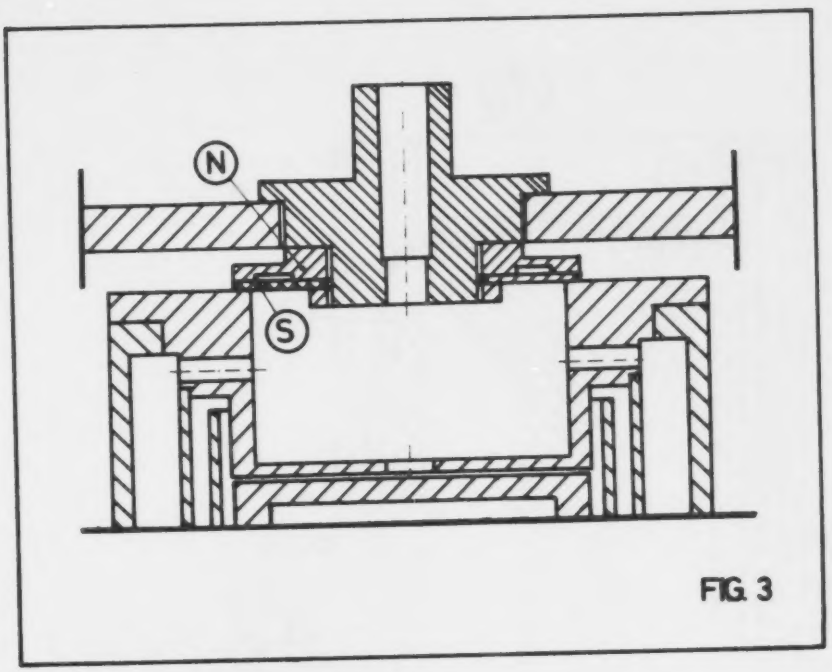

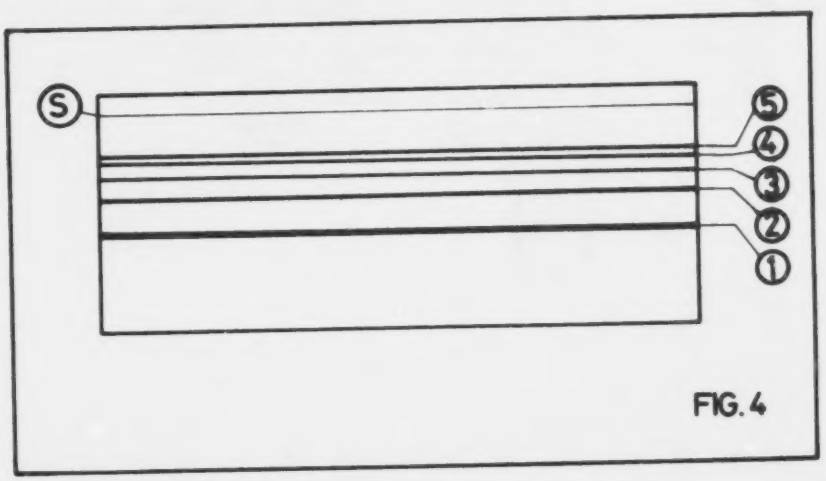

Fig.3: Head of rotor I with gasket. N, nylon spring disc. S, teflon sheet.

Fig.4: Latex aerosol deposits on collection foil. S, projection of the slit. 1), single spheres.2) to 5),aggregates ot two, three, four and five spheres.

outer wall of the measuring chamber, the upper wall of the aerosol slit and the cleaning system, from the base plate, B, which is fixed to the inner parts of the rotors. In the first rotor (see fig. 1) the removable piece is bolted to the base plate by six bolts and it is positioned by a very narrowly spaced cylindrical guide, whereas in the second rotor the parts are connected by a large thread and held in position by a conical guide.

For measuring the rotational speed, the first rotor is equipped with ten small permanent magnets in the top of the rotor. The magnets pass beneath an electromagnetic pick up in the housing of the centrifuge. The top of the second rotor bears a disc with twelve blank fields on a dark background, for switching a photo transistor. Primarily, the rotors have not been designed for direct measurements of flow rates. This inability became a serious draw back during a certain period of the work, and therefore the first rotor has been equipped with a seal in order to enable the measurement of the total flow rate. This seal, which is fixed to the housing of the centrifuge, consists essentially of a nylon spring disc and of a teflon sheet which is pressed to the top of the rotor (see fig.3). The seal is tight, up to rotational speeds of 6ooo rpm. The flow rates are measured by means of a soap film moving in a calibrated glass tube mounted on top of the housing. (It should be mentioned, that the teflon sheet undergoes heavy wear by the rotor, and therefore must be replaced frequently).

Particle size analysis

The aerosol slit has a width of o,1 mm which is small compared to the chamber width of 3 mm, i.e. the distance between the inner wall and the outer wall of the chamber. The aerosol particles therefore start their movement to the outer wall from fairly equivalent positions at the end of the slit. Consequently the particles of an extremely monodispersed aerosol will occur at similarily equivalent deposition locations, which after unrolling the foil appear as a straight line parallel to the projection of the slit. The deposits of a latex aerosol, which contains a number

of different, aerodynamically separated classes of particles (15), (19), (21), thus appear as a set of separated lines (see fig. 4), and after counting as a set of separated number size distributions (see fig. 5). The distance between these lines and the projection of the slit is introduced as the deposition length, L_p, of the particles.

From the point of an observer rotating with the chamber, the particle velocity has essentially two components, i.e. the radial velocity, v_r, in the radial direction, and the velocity, v_z, in the axial direction. The azimuthal velocities of the particle vanish, if solid body rotation is assumed for the gas and the particles. The influence of the centrifugal force on the movement of the particle follows from STOKES' law, which may be accepted in the form

$$(\pi/6).D_p^3.\rho_p.\omega^2.R = 3.\pi.\eta_g.D_p.v_r'/B_{pg} \qquad (1)$$

for spherical particles of diameter D_p, and density, ρ_p. The slip correction factor, B_{pg}, is given by

$$B_{pg} = 1 + (\lambda_g/D_p).(1{,}36 + 0{,}7.\exp(-3{,}68(\lambda_g/D_p)) \qquad (2)$$

The gas has the viscosity, η_g, and the mean free path, λ_g, of the molecules.

The velocity, v_r', is the relative velocity of the particles in the gas, in the radial direction. But because of the cylindrical design of the rotor, the gas does not possess radial velocities within the measuring chamber, and consequently the radial velocity, v_r, of the particle and its radial velocity, v_r', relative to the gas, are identical. This leads to the equation

$$v_r = (B_{pg}.D_p^2.\rho_p/18.\eta_g).(\omega^2.R) \qquad (3)$$

for the radial velocity of the particle.

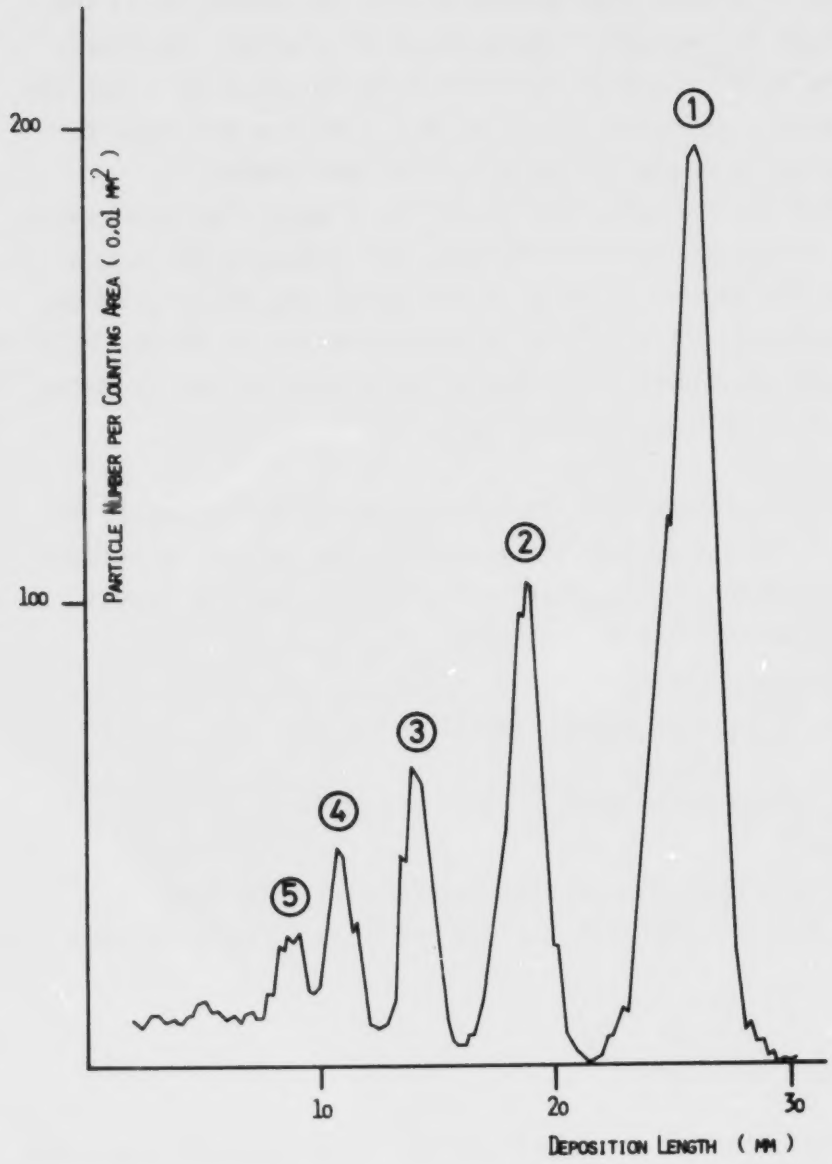

Fig.5: Number size distribution of latex aerosol. 1), single spheres; 2) to 5), aggregates of two to five spheres.

The acceleration $\omega^2.R$ needs some consideration. The radius, R, is the radial distance of the particle from the axis of rotation. Thus the acceleration increases as the particle moves to the outer wall. But the variation of this radial distance, R, is ΔR = 3 mm from the inner to the outer wall, which is small compared to the mean radius $\bar{R} = (R_o + R_i)/2 = (4o + 37)/2 = 38{,}5$ mm of the chamber. The acceleration is transmitted to the particles by the gas, and therefore the angular velocity, ω, is the angular velocity of the gas at the position of the particles. In general, there will be an angular motion of the gas relative to the rotor, and consequently the angular velocities of the gas differ from the angular velocity, ω_o, of the rotor.

Fortunately, the solution of these problems is fairly simple, if the assumption is justified that the gas within the centrifuge rotates like a solid body with an velocity ω_o. In this case the radial velocity of the particles is determined by

$$v_r = (B_{pg}.D_p^2.\rho_p/18.\eta_g).(\omega_o^2.\bar{R}) \qquad (4)$$

with a constant acceleration term $\omega_o^2.\bar{R}$ for all particles.

It should be mentioned here, that particles with the same $D^* = D_p.(B_{pg}.\rho_p)^{1/2}$ are obviously not discriminated by the centrifuge. The equation

$$D_p^* = D_p.(B_{pg}.\rho_p)^{1/2} \qquad (5)$$

is therefore introduced as definition for the aerodynamic equivalent size of a particle, and it is this parameter, which is directly related to the radial velocity of the particle.

During their way from the inner wall to the outer one, the particles are transported downstream together with the gas. The assumption is justified that the axial velocities of the gas and the particles are identical and therefore the particle velocities will show the same velocity profile as

the gas velocities. But STÖBER et al. (22) have proven that the deposition length, L_p, of a particle is independent of the true path of the particle; rather the deposition length is determined by the average axial velocity, $\bar{v}_z$,

$$\bar{v}_z = Q/(\pi.(R_o^2 - R_i^2)) = Q/(2\pi.\bar{R}.\Delta R) \qquad (6)$$

Regarding the path of a particle, one finds that within the same period of time the particle has travelled the distance, ΔR, radially, and the deposition length, L_p, axially, and consequently the relation

$$L_p/\Delta R = \bar{v}_z \; / \; \bar{v}_r \qquad (7)$$

holds, where $\bar{v}_r$ is the average radial velocity of the particle on the path to the outer wall. Replacing of $\bar{v}_z$ by equation (6) and $\bar{v}_r$ by equation (4) yields the equation (8) for the deposition length, L_p,

$$L_p = o,8959.1o^{-6}.(Q/D_p^{*2}.N^2) \qquad (8)$$

where ω_o^2 has been replaced by $4.\pi^2.N^2$ and η_g by its numerical value at standard temperatures. (It should be mentioned, that the exact calculation of the deposition length would change the constant from k = o,8959 to k = o,8963 (19)).

However, equation (8) is based on the assumption that the gas rotates like a solid body with angular velocity ω_o. A direct proof by measuring the angular velocities of the gas is difficult, but the observations with latex particles of well known size indicate that this assumption is justified. First, the calibration curves, i.e. the empirical relations between the sizes of the latex particles and their deposition lengths follow equations like

$$L_p = A_i.(D_p^*)^{-2} \qquad (9)$$

where the constants, A_i, depend on the flow rate, Q, and on the rotational speed, N. These equations coincide perfectly with equ. (8) as far as particle size and deposition length is concerned. By comparing (8) and (9), the relation

$$A_i = 0{,}8959.10^{-6}.(Q/N^2) = k.(Q/N^2) \qquad (10)$$

follows, which immediately leads to the equation

$$L_p^* = (D_p^*)^{-2} = (1/k).(L_p.N^2/Q) \qquad (11)$$

where the inverse square of the equivalent size has been introduced as the reduced deposition length, L_p^*. By means of (11), the reduced deposition length and therefore the equivalent size of the latex particles is completely determined by the data of the centrifuge, i.e. the deposition length, the flow rate and the rotational speed. Other values for the equivalent sizes of the same particles are calculated from their known diameter using equ. (5). Both methods should be in agreement if the assumption of solid body rotation is correct for the particle motion.

The results of confirming experiments are listed in table I. Four different latex particle sizes have been used, i.e. D_p = 1,305 µm, D_p = 0,79 µm, D_p = 0,557 µm and D_p = 0,357 µm. A density of 1,05 has been assumed for these particles. The deposition lengths, L_p, have been measured for different rotational speeds and different flow rates. From these data, the reduced deposition lengths, L_p^*, have been calculated according to equ. (11). For a given latex size these values are in fair agreement, and the average reduced deposition length, $\bar{L}_p^*$, has been used for calculating the equivalent sizes, $\bar{D}_p^*$, of the latex particles. These sizes are in agreement with the equivalent sizes, D_p^*, calculated from the latex diameters as quoted by the manufacturer. The relatively large deviations for latex particles of 0,790 µm diameter indicate, however, that the quoted size might be wrong.

The data of table I represent nine different calibration curves. These curves should coincide to a single curve, when the reduced deposition lengths are introduced according to equation (11). Its logarithmic form is given by

$$\ln L_p^* = 2.\ln D_p^* \qquad (12)$$

where L_p^* stands for the reduced deposition lengths calculated from the centrifuge data, and D_p^* for the equivalent size calculated from the diameters quoted by the manufacturer. The graph of this curve, which is represented in fig. 6 together with the experimental data, indicates very clearly the consistency of theory and experiment for three of the latex sizes.

Operational features of the ROSL spectrometer

The aerosol flow limiting orifice restricts the flow into the aerosol slit. Depending on the cross section of this orifice, the aerosol flow is low for small orifices and vice versa. The influence of the AFLO orifice on the resolving power of the centrifuge is of more importance. With smaller orifices the aerosol layer entering the measuring chamber is narrowed and consequently the initial positions as well as the deposition locations of the particles are better defined. This effect is demonstrated by the variance of the deposit locations of single latex spheres, which have been collected with different AFLO orifices. As demonstrated in fig. 7, the variance decreases with diminishing orifice cross sections. A further, though minor decrease could be expected for still smaller orifices, but for such experiments long collection periods are needed, which increase the errors due to variations of the rotational speed and other long term instabilities.

Some experiments have been conducted to determine the resolving power of the aerosol spectrometer, at low aerosol flow conditions. The number size distributions of the latex aerosols are assumed to be Gaussian. Then the variance, V_m, of the observed size distribution is the sum of the

TABLE 1. ANALYSIS OF LATEX PARTICLE DEPOSITS.

N	Q	D_p = 1,3o5 µm L_p	L_p^x	D_p = o,79o µm L_p	L_p^x	D_p = o,557 µm L_p	L_p^x	D_p = o,357 µm L_p	L_p^x
3ooo	19,3	o,37	o,535	o,87	1,259	1,77	2,559	4,oo	5,783
3ooo	31,5	o,59	o,523	1,375	1,218	2,82	2,498	6,o2	5,333
3ooo	49,5	o,9o9	o,512	2,15	1,212	4,6o	2,593	--	--
48oo	35,8	--	--	o,62	1,237	1,28	2,554	3,12	6,225
48oo	55,o	o,4o	o,52o	o,95	1,234	2,oo	2,598	4,41	5,728
48oo	75,o	o,51	o,486	1,35	1,286	2,61	2,486	6,35	6,o48
6ooo	47,5	--	--	o,52	1,222	1,o9	2,561	2,35	5,522
6ooo	71,5	o,33	o,515	o,81	1,264	1,57	2,451	3,6o	5,62o
6ooo	1o9,o	o,49	o,5o2	1,22	1,249	2,5o	2,56o	5,55	5,683
		Γ_p^x = o,513		Γ_p^x = 1,242		Γ_p^x = 2,54o		Γ_p^x = 5,743	
		$\bar{D}_p^x$ = 1,396 µm		$\bar{D}_p^x$ = o,897 µm		$\bar{D}_p^x$ = o,627 µm		$\bar{D}_p^x$ = o,417 µm	
		D_p^x = 1,4o1 µm		D_p^x = o,87o µm		D_p^x = o,629 µm		D_p^x = o,42o µm	

D_p, quoted diameter; D_p^x, equivalent size, calculated from D_p; Γ_p^x, reduced deposition length(μm^{-2}), measured by the centrifuge; $\bar{D}_p^x$, equivalent size, calculated from Γ_p^x. Q:cm^3/sec; N:1/min;L_p:cm

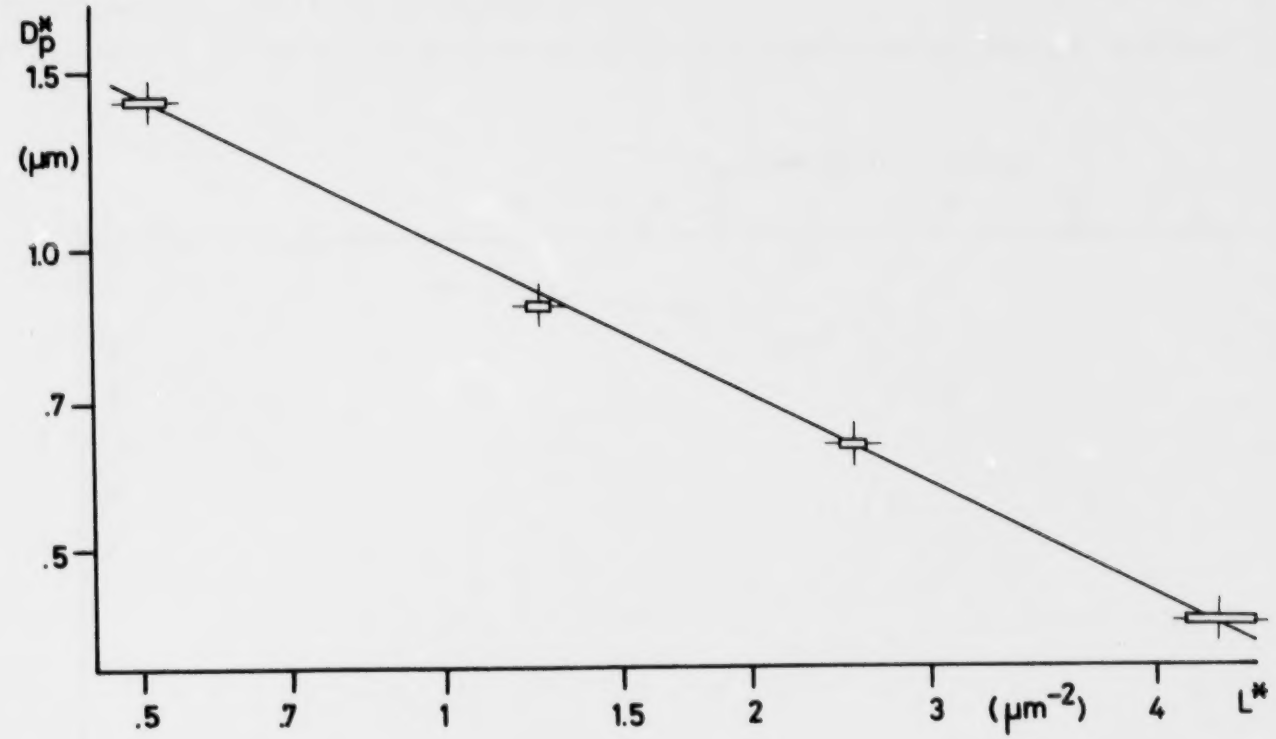

Fig.6: The reduced deposition length and its relationship to the equivalent particle size, calculated from DOW quotations. Bars indicate the average and the range of the experimental data, the solid line represents the theoretical expectation.

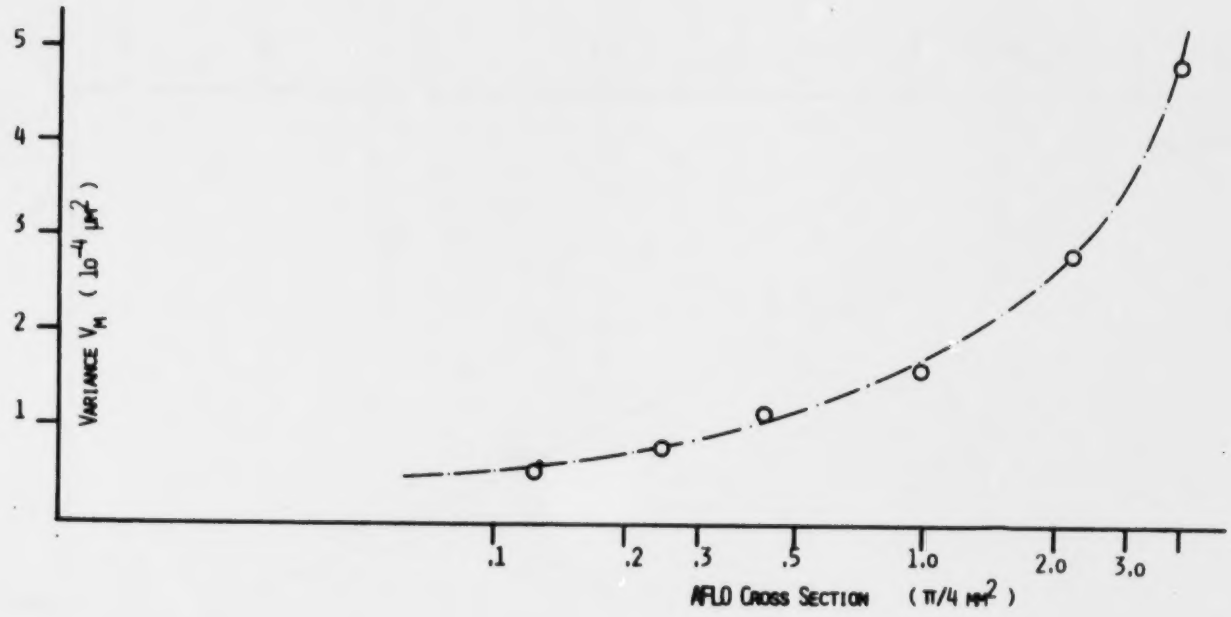

Fig.7: Variance of number size distributions of single latex particles and its relationship to the cross section of the AFLO orifice.

variance, V_o, of the original size distribution (quoted by the manufacturer), and of the variance, V_i, added by the centrifuge:

$$V_m = V_o + V_i \qquad (13)$$

The contribution of the instrument could then be estimated from equ.(14)

$$V_i = V_m - V_o \qquad (14)$$

The data show, however, that this method is not consistent because of inaccuracies of the original variances, V_o. Two examples may demonstrate the difficulties. The latex particles of o,557 µm diameter have an original variance of V_o = 1,1664.1o^{-4} µm^2, whereas the measured variance has a value of V_m = o,7225.1o^{-4} µm^2. Consequently, the contribution of the instrument would be negative, V_i = -o,4439.1o^{-4} µm^2. The latex particles of o,79o µm diameter have anoriginal variance of V_o = o,1936.1o^{-4} µm^2, whereas a value of V_m = o,5373.1o^{-4} µm^2 has been found by the centrifuge. In this case, the contribution of the instrument would be V_i = o,3436.1o^{-4}µm^2. The occurancesof negative variances demonstrate the infeasability of the procedure, and it is therefore not adequate to draw quantitative conclusions even on the positive data. However, the statement holds, that the variance contributed by the centrifuge is of the same order of magnitude or less than the variance of the latex particles, for high resolving conditions (2o),(19).

The highest aerosol flow rate and the lowest resolving power is obtained when the rotor is operated with no AFLO orifice in the center of the slit. In this case, the number size distributions of single latex spheres exhibit a rectangular shape. In addition, the size distribution of the different components of the latex aerosol, i.e. the singlet, doublet and the other multiple particles, may overlap considerably. As shown by the number size distribution in fig. 8, the rectangular shape develops from larger to smaller deposition lengths. Therefore the narrow distributions and the wide ones coincide at the descent to smaller particles. In order to achieve classification, the flow has to be laminar and

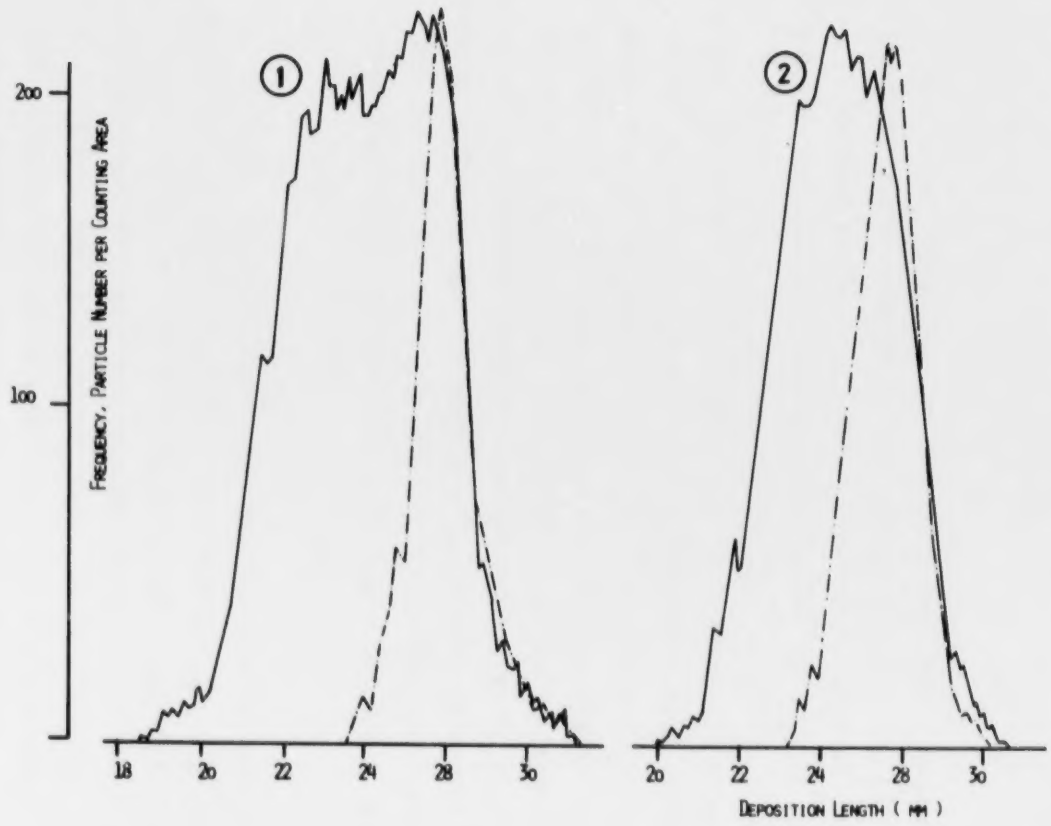

Fig.8: Number size distributions of single latex spheres at different AFLO cross sections. Particle size o,557 µm diameter. Small cross sections, dashed lines. Large cross sections, solid lines. 1), 6ooo rpm and 4,7 mm^2 TFLO. 2), 5ooo rpm and 11,8 mm^2 TFLO.

vortex-free within the chamber. Such conditions are set by the TFLO in the base plate of the rotor. Good flow conditions are indicated by straight and narrow deposition lines, if latex aerosols are used. At unsuitably high flow rates, however, the latex deposits exhibit a regular, sinusoidal structure, and in extreme cases a regular array of overlapping arcs. The TFLO are used to set the measuring range of the centrifuge. Because of the definite length of the chamber, the deposition lengths, L_p, are restricted to values between L_p = o cm and L_p = 11,o cm. However, the usefull range for data analysis is smaller. Near the slit at L_p = 0, the particle sizes crowd together, and the sensitivity, $\Delta L_p/\Delta D_p$, is almost zero. Therefore, deposition lengths below o,3 cm or o,5 cm do not bear much information on the difference of particle sizes. With increasing deposition lengths, the sensitivity grows continuously, according to equ. (9)

$$\Delta L_p/\Delta D_p^* = -C.(L_p)^{1/2} \qquad (15)$$

where C is a constant parameter. But on the other hand the concentrations of the deposits decrease reciprocally, with the consequence of higher statistical errors. Moreover, the flow pattern at the end of the chamber may be disturbed by the outgoing flow. For these reasons it is not advisable to extend the range of evaluated deposition lengths beyond L_p = 8 cm or L_p = 9 cm. This range of deposition lengths comprises about half an order of magnitude in particle size, according to equ. (9). This is a fairly narrow measuring range, and should therefore be adjusted carefully to the particle sizes of main interest. This is achieved by the appropriate choice of the TFLO and of the rotational speed. As a rule, the particles of main interest, e.g. the peak of a monodispersed aerosol, should be deposited at deposition lengths between L_p = 2 cm and L_p = 5 cm (see fig. 9, 1o).

For a given rotational speed, the total flow rate increases when the total orifice cross section, i.e. the sum of the TFLO cross sections, is enlarged. Therefore a certain calibration of the centrifuge is finely adjusted by using TFLO of different sizes. It should be mentioned, however, that the flow rate may be ambivalent for certain TFLO orifice combinations. This fact is illustrated in fig. 11. According to the graph the flow rate

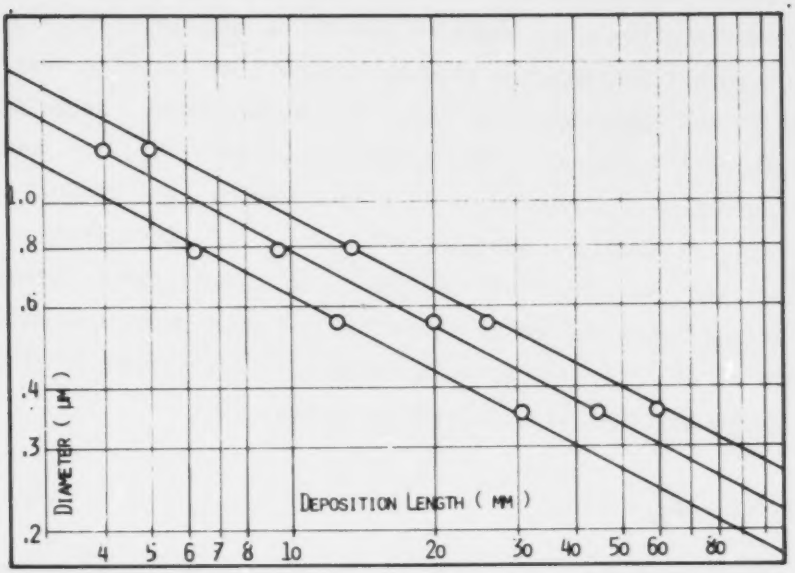

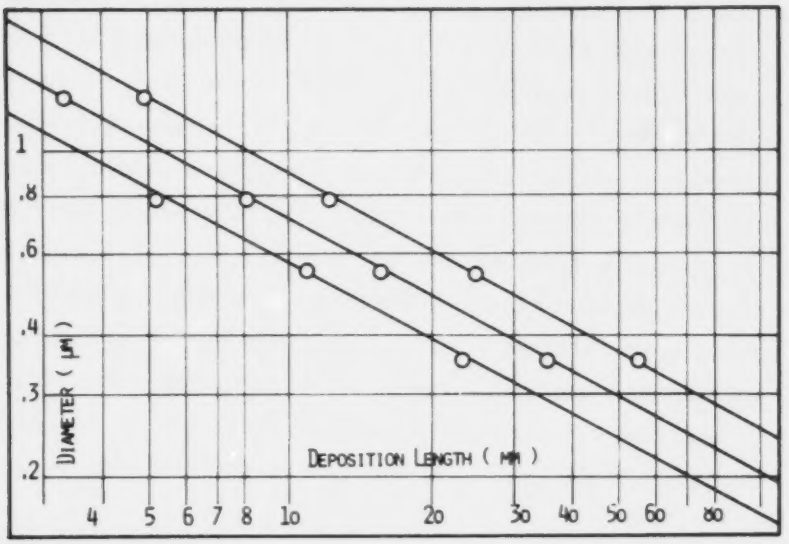

FIG.9 (ABOVE)

FIG.10(BELOW)

Fig.9: Calibration curves. Rotational speed 48oo rpm; TFLOs 2,36 mm^2 (lower curve), 4,71 mm^2 (middle curve), 11,78 mm^2 (upper curve).

Fig.1o: Calibration curves. Rotational speed 6ooo rpm. TFLOs 2,36 mm^2(lower curve), 4,71 mm^2 (middle curve), 18,85 mm^2 (upper curve).

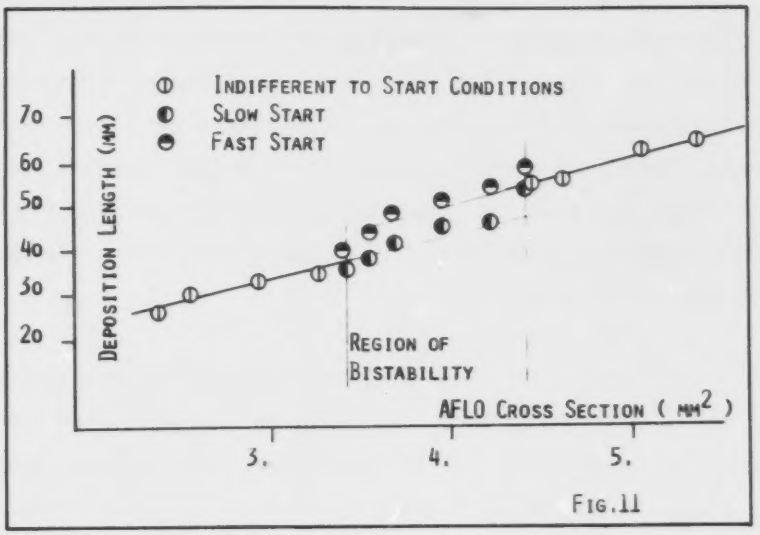

FIG.11

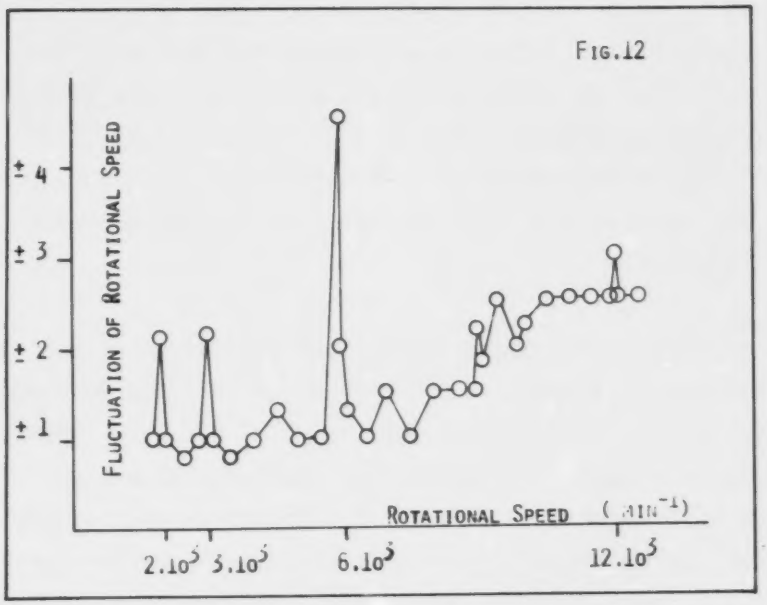

Fig.11: Ambivalent deposition lengths. 4800 rpm, 0,557 µm latex size.

Fig.12: Range of speed fluctuations for the system rotor II/regulated power supply.

is ambivalent in a limited domain of total orifice cross sections, and the actual value of the flow rate depends on the mode of accelerating the rotor: a "fast" start will yield the higher flow rate, whereas a "slow" start produces the lower flow rate. This behaviour is effected by the TFLO orifices and their arrangement in the rotor base. Ambivalence occurs for certain orifice sets with three orifices of one size and the other three of another size, but only if these orifices are arranged alternately, i.e. each orifice being neighboured by orifices of the other size (19).

During operation, short term and long term fluctuations of the rotor speed must be taken into account. The motor is a high speed collector motor, and it is operated from the power line of the laboratory. The motor speed is usually set by the voltage of an variable autotransformer. In long term operation, the warming up of the rotor is a further source for speed fluctuations. In order to overcome these deficiencies, a speed controller has been developed, which keeps the rotational speed within the limits of a few rotations per minute. Typical short term fluctuations are less than $\pm$ 2 rpm, but, as shown by fig. 12., there are a few points of lower stability, where the fluctuations are as high as $\pm$ 1o rpm. The long term stability measured for hours of continuous operation is better than o,5 %, i.e. the measured speed does not deviate more than 1o rpm from any preset value between 2ooo rpm and 12ooo rpm.

Another effect of long period operations is the warming up of the rotor by the heat of the bearings. Temperature differences of $1o^{o}C$ and $2o^{o}C$ above room temperature have been observed at the outer side of the rotor. Consequently the inner parts should be warmer, and temperature gradients across the measuring chamber are to be expected. Fortunately, the inner wall of the chamber is warmer than the outer wall, and therefore the temperature gradients is in favour of a stable stratification of the flow. However, the gas inside the chamber is altered in density and viscosity, and consequently changes of the flow rate could occur. The experiments show that such changes in calibration are negligible. Latex aerosols have been collected on the same foil for a cool and a warm rotor. As fig. 13 demonstrates, there is no significant difference in flow rates between a cool and a warm rotor.

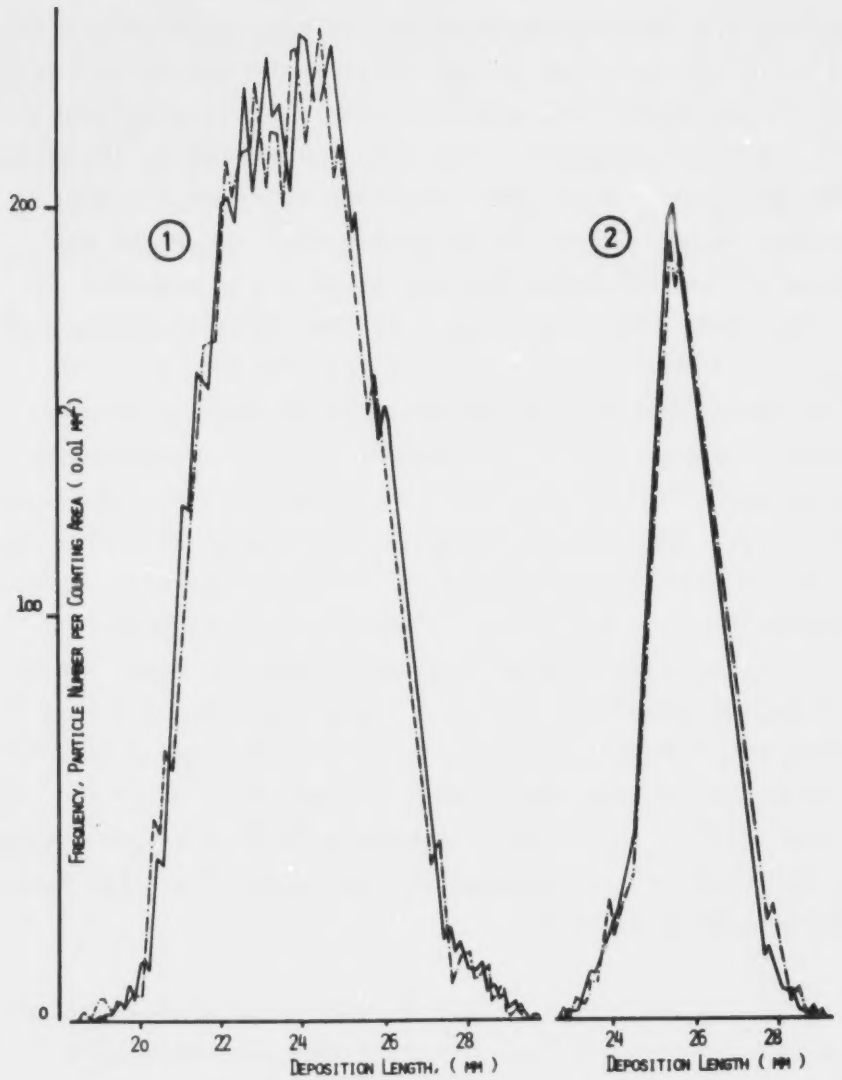

Fig. 13: Number size distributions of single latex particles for cold (solid line) and warmed (dashed line) rotor I. 1), 6000 rpm, AFLO 3,14 mm^2, TFLO 18,8 mm^2. 2),5000 rpm, AFLO 0,09 mm^2 TFLO 18,8 mm^2. Particle size 0,557 µm diameter.

Discussion

As indicated by the calibration curves of the ROSL spectrometer the angular velocities of the particles do not differ significantly from the angular velocity of the rotor. This property opens a way to precision measurements of aerodynamic diameters. The precision depends on the errors in measuring the deposition length, the total flow rate, and the angular velocity. The errors in the deposition length are about 0.1 mm at the large particle end of the deposition foil and about 0.3 mm near the small particle end. These errors could still be lowered by elaborate measuring techniques, however, care must be taken that the foil is smooth and perfectly contacting the wall during operation in order to prevent flow disturbations. The precision of the angular velocity measurements is sufficient, the velocity is easily measured and well controlled by the regulated power supply. Precision measurements of the total flow rate are a serious problem. In order to use external flow meters the rotor is to be connected leakageless to the housing. Solutions as represented for rotor I are not satisfactorily because they do not work at higher rotational speeds and they do not allow continuous functional control during operation. Probing the flow with particles of well known sizes poses the problem of the precision of size measurements. As demonstrated by fig. 13a the scatter of the particle size data is unacceptable for precisely determining the calibration curves, and consequently the total flow rates would be submitted to the same uncertainty.

The capacity of the centrifuge to work at speeds up to 12ooo rpm or more is still unused. Experiments have been performed successfully in collecting small sized Latex aerosols near the slit. Classification turned out to be perfect justifying the conclusion, that particles with sizes around 0.05 μm could be sized.

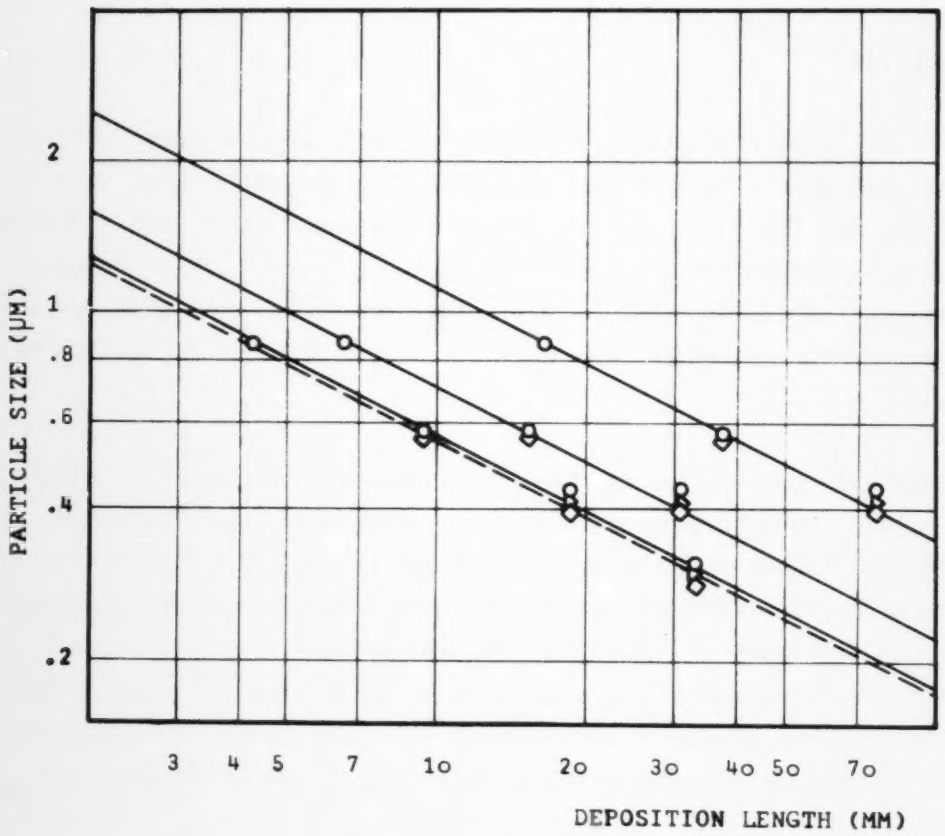

Fig 13a : Calibration curves for rotor II. 5ooo rpm and TFLO 1o,6 mm^2 (upper curve) , 5ooo rpm and TFLO 4,7 mm^2 (middle curve), 9ooo rpm and TFLO 4,7 mm^2 (lower curves, dashed and solid). ○ sizes by DOW, ◇ sizes by (53), ▷ sizes by (54).

THE DIFFUSION BATTERY

Introduction

Aerosol particles undergo BROWNian movement, which causes them to migrate through the gas. If they meet a surface they will stick to it and never rebound. The chance for a particle to be deposited on walls depends on particle size and on the dimensions of the container, once the gas, its temperature and its pressure is given. The smaller the particles are and the narrower the container, the higher are the chances for deposition by diffusion.

TOWNSEND (23) in 19oo was the first to derive an analytical equation which applies to diffusion deposition in cylindrical tubes. Later on, GORMLEY and KENNEDY (24) and many others worked out similar solutions of this problem. Progress with respect to certain corrections has been made by the use of computers (TAN (25), TAN and HUE (26)). But diffusion is not always the sole mechanism for deposition in tubes. Sedimentation within the tubes and impaction and interception at the entrance must be taken into account, especially for particles of more than o,1 µm in diameter.

Many investigations have been performed in order to solve these problems theoretically, but the results are to some extent in disagreement. Therefore it has been the goal of this work, to study the effects of impaction and interception experimentally, by applying a diffusion battery and the ROSL aerosol spectrometer to monodisperse NaCl aerosols.

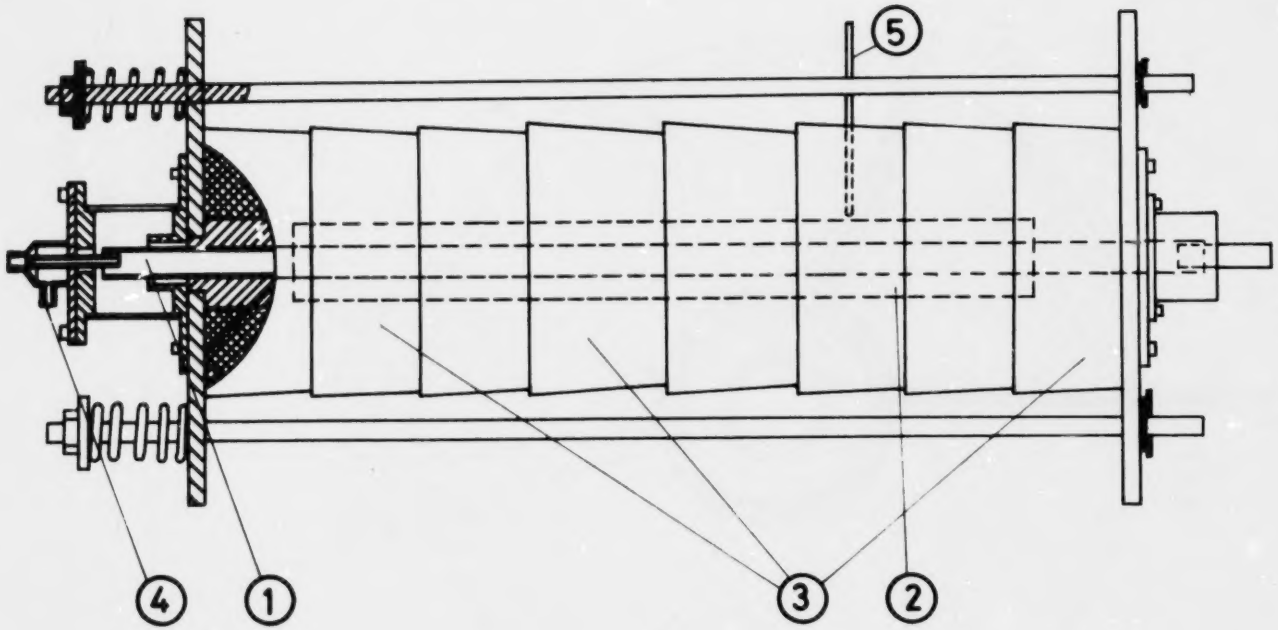

Fig.14: Furnace for the generation of monodispersed NaCl aerosols. 1), center tube for the production of aerosols; 2), heaters; 3), thermal insulation (fire bricks);4),ejector for the dilution of the aerosols; 5), thermo couple.

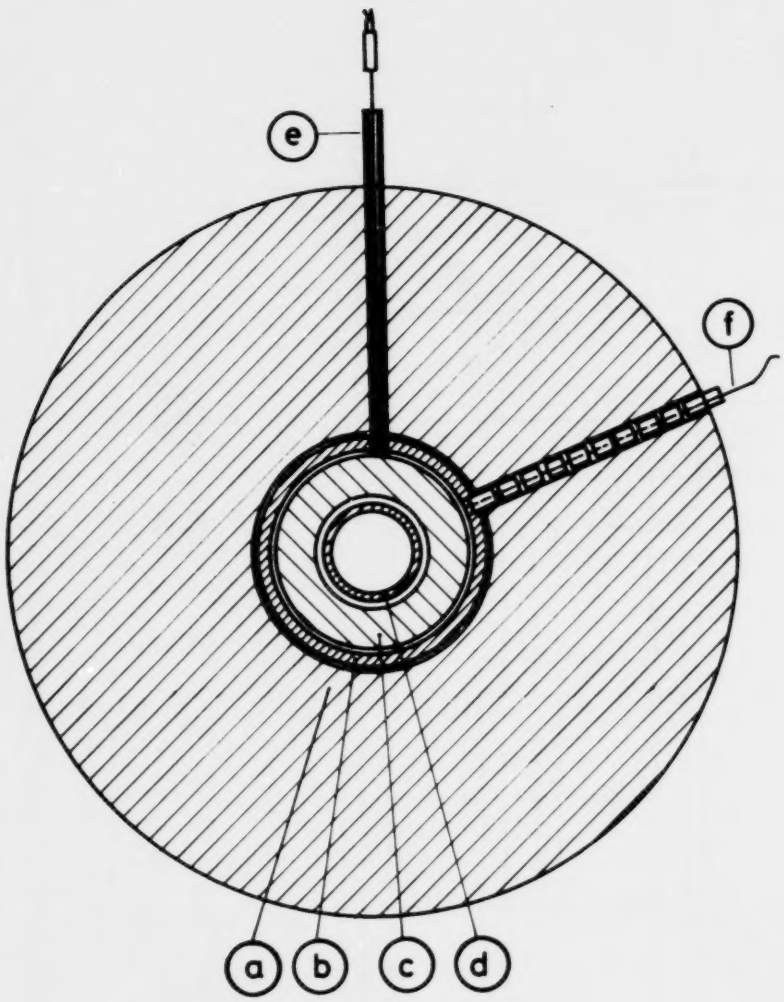

Fig.15: Cross section of the aerosol generator at the position of a heater element. A, fire bricks.B, ceramic tube for sheltering the heating wires. C, ceramic tube for carrying the heating wires. D, center tube for aerosol production. E, thermo couple. F, heating wire lead.

The earlier classifiers by diffusion, i.e. the diffusion batteries, were made from bundles of long and narrow tubes or from packages of sturdy plates with narrow spacings. The large draw back of such batteries was their bulkiness and weight. Recently SINCLAIR (27) described a handy diffusion battery which he has used in field work. For this battery thin plates with a large number of extremely fine, collimated holes (collimated hole structures = CHS) have been used. MATTESON et al. (28) specified another diffusion battery with CHS plates, where the plates had about $3.1o^5$ holes of 15 µm diameter. A similar battery of six, nominally identical CHS plates has been used for this work (29) (3o).

A special generator for the NaCl aerosol has been developed. The generator can produce fairly monodispersed aerosols in the desired particle size range (3o), (31).

The NaCl aercsol generator

The generator is a tube furnace with a center tube of approximately 1,5 m length. Different tubes have been used, with 3 cm o.d. and 2,7 cm i.d., or 2,5 cm o.d. and 2,o cm i.d.. The center tubes are made from pure aluminium oxide which is highly resistant to attack by NaCl vapors. The center tube is surrounded by other ceramic tubes which carry three seperated heaters. These heaters which could be operated up to $1ooo^oC$ have lengths of 2o cm, they are arranged serially with distances of 2o cm between them. They are electrically independent thus forming three independent heating zones. The heaters are protected by a third ceramic tube. Finally, the whole tube system is imbedded in thick fire bricks for thermal insulation (see fig. 14 and fig. 15). The bricks are resting on iron rods, and the furnace is hold together by two springloaded end plates which carry special flanges for the aerosol and the gas ports. The aerosol port is equipped with an ejector for rapid dilution of the aerosol. The seal between the center tube and the flanges is made by a silicone elastomer, which possesses some flexibility after hardening. The center tube undergoes extension and bending by heating and therefore cannot be connected rigidly to the ports.

The electrical power of each heater is controlled by thermostats, specifically PLASTOMATIC SCR by PHILIPS. The reference temperatures are measured by three thermocouples just above the heaters in the middle of each zone. These temperatures are lower than the gas temperatures in the center tube, and a calibration is needed to relate the gas temperatures to the reference temperatures of the thermostats. Such calibration curves are shown in fig. 16 for two different tubes. In these calibrations, the highest gas temperatures of the heating zones are indicated. Temperature profiles along the center tube are shown in the next figures. The temperature profiles are slightly different for a stagnant and for a streaming gas, at a flow rate of 1 l/min. A downstream shift is observed, and a slight decrease of the highest temperatures, but these changes are negligible (see fig. 17). The temperature profiles are time dependent. Observations demonstrate that the highest temperatures are reached fairly quickly and no significant increase is found after a time lapse of one hour from the start of heating. In the valleys between the heating zones, however, changes are observed up to 18 hours after heating commences (see fig. 18).

For aerosol production, ceramic boats are placed in the center tube. The zone next to the gas port, i.e. zone I, contains a boat filled with NaF for nuclei production. Zone II contains one or two boats with NaCl for aerosol production. Zone III at the end of the generator is left free. Nitrogen, which is carefully dried in some applications, has been used for carrier gas.

A drawback of the furnace is the frequent rupture of the center tube. Thermal stresses due to the high temperature gradients along the tube are a main source, but the influence of the NaCl and NaF vapours should not be neglected. The risk of breakage increases when cold boats are placed in the furnace. The problem is still far from being solved satisfactorily. Thin walled aluminum oxide tubes seem to stand longer than thick walled ones; steel tubes and quartz tubes will disintegrate within days.

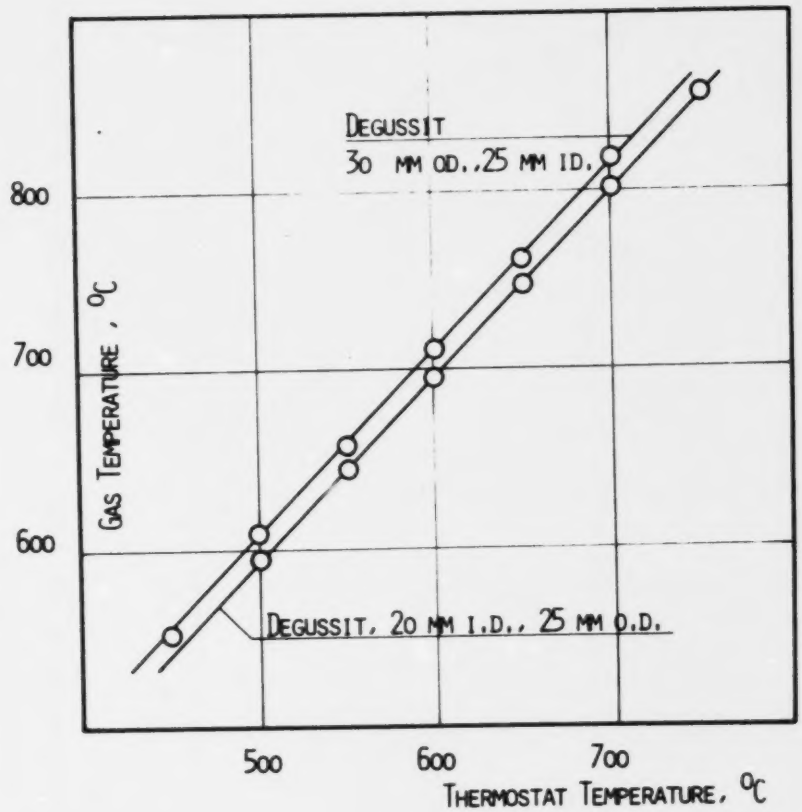

Fig.16: Calibration curves relating the temperatures in the center tube to the temperatures of the thermostats.

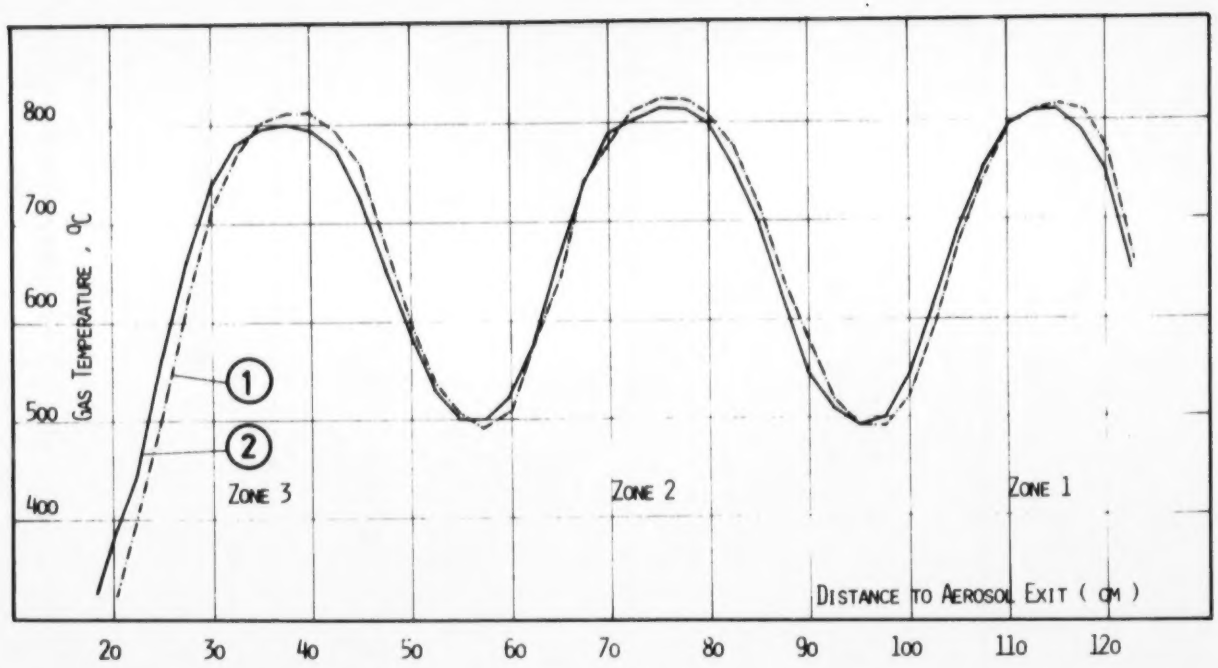

Fig.17: Gas temperatures along the axis of the center tube at different flow rates. Curve 1), zero flow rate; curve 2), 1 l/min .

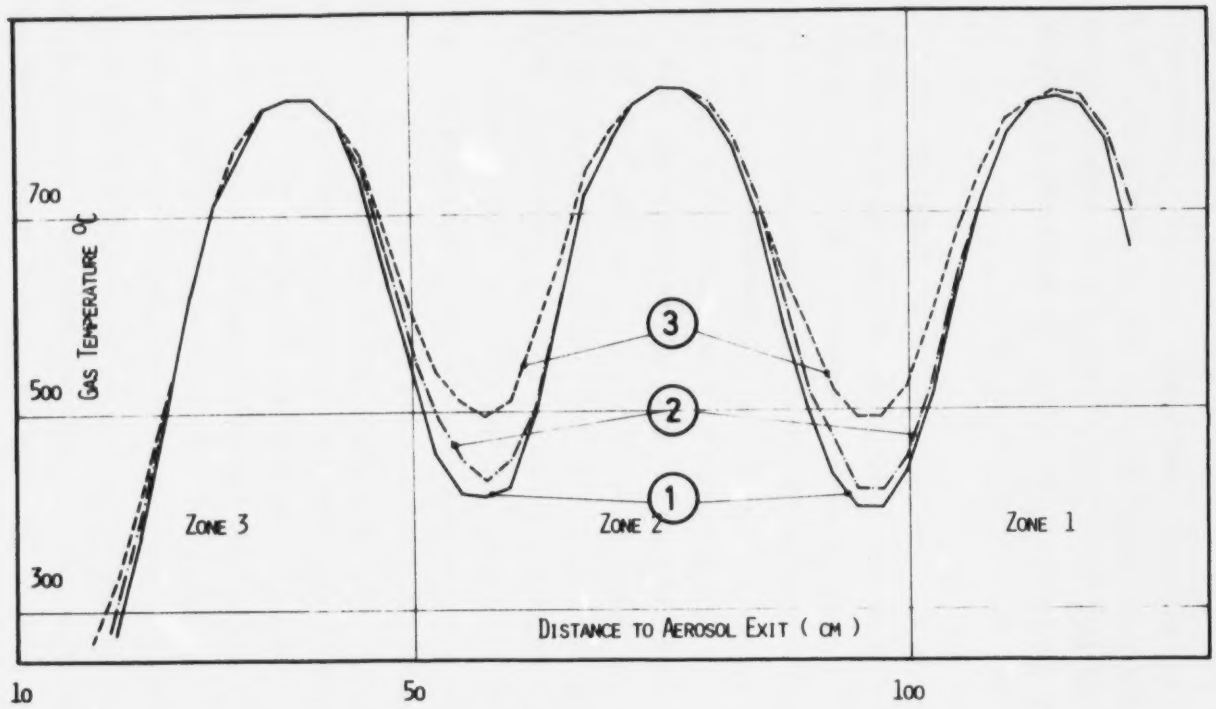

Fig.18: Gas temperatures along the axis of the center tube, at zero flow rates and different time lapses after starting the generator. Curve 1), time lapse of one hour ; curve 2), after three hours, and curve 3), after eighteen hours.

The NaCl aerosols

The aerosols produced by the generator are fairly monodisperse. When illuminated with a beam of white light they exhibit a sequence of definite colours in the scattered light, from the red to the yellow, the green and the blue. Not only does this phenomenon, i.e. the higher order TYNDALL spectra, indicate good monodispersity, but it permits the continuous monitoring of the particle size by measuring the angular position of a given colour, e.g. the red (29). This size measurement represents an optical equivalent diameter of the aerosol.

The aerosol production depends on three parameters, i.e. the temperature, T1, of the NaF source, the temperature, T2, of the NaCl source, and the flow rate, Q. The temperature, T1, influences the size and the monodispersity of the aerosol. For high temperatures the nuclei contribute considerably to the mass of the aerosol particles and therefore the size increases when the temperature is raised beyond a certain level. For lower temperatures, the nuclei do not contribute to mass, and therefore the particle size becomes independent of the temperature at the NaF boat. The limit between these two regimes is about $55o^{o}C$ (see fig. 19). The monodispersity, which decreases for high and for low temperature, is best at temperatures of about $6oo^{o}C$. The main purpose of heating the NaF source is the production of condensation nuclei. The tube itself produces some nuclei, but these are insufficient in number or perhaps inadequat in kind to effect the condensation of monodispersed aerosols. With the NaF source, nuclei concentrations of the order of $1o^{6}$ to $1o^{7}$ per cc are obtained. These nuclei concentrations are almost insensitive to changes in temperature, T1, at the NaF boat. It should be mentioned that the NaF boat becomes unnecessary after an interval of operation, after which it does not alter the efficiency of the nuclei production. Nuclei are presumably produced from contaminations at the walls. The temperature, T2, of zone II determines by evaporation the amount of NaCl which condenses on the nuclei, and therefore this temperature dominates the size of the aerosol. The relation between size and temperature, T2, is fairly reproducible, if certain rules are obeyed. First, the procedure of exchanging the NaCl boats should be performed very carefully to minimize

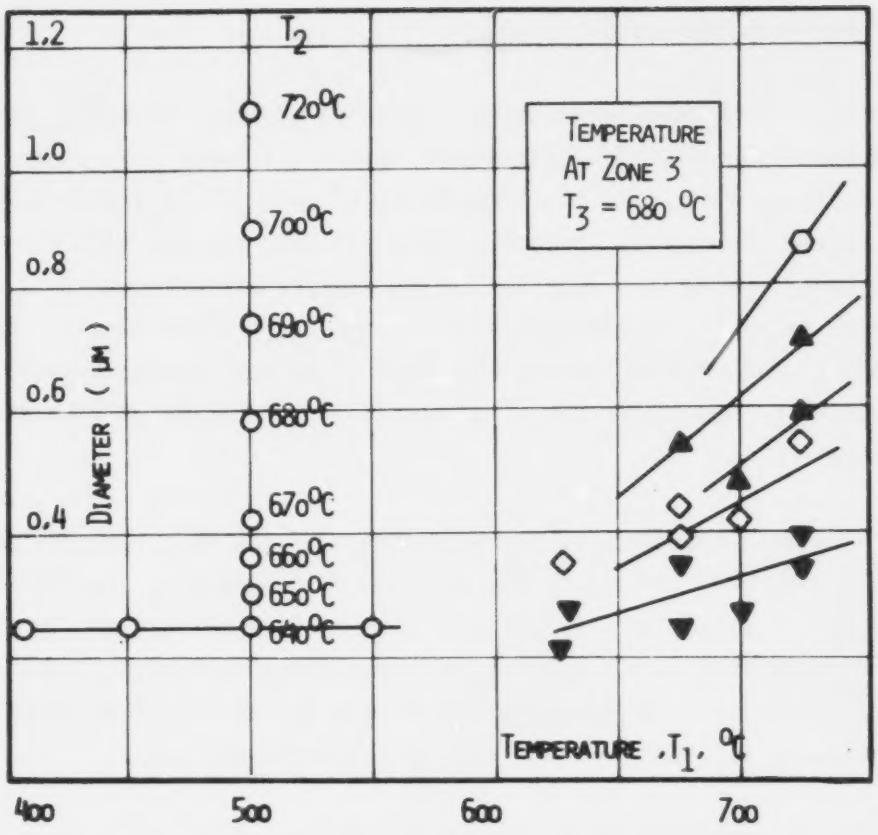

Fig. 19: The sizes of the monodispersed NaCl aerosols in dependence of the temperatures at zone I and zone II.

contamination introduced by the boats. Secondly, after a change of the thermostat temperature, the furnace is out of equilibrium for one hour, during which time the average size of the aerosol is unstable. Finally, the furnace should be conditioned ahead of longer periods of stand by under power, i.e. the NaCl boats are to be removed from the furnace, and the tube is to be flushed with clean gas for a couple of hours to evaporate salt remnants from the heating zones.

Zone III, which does not contain a material source, influences the degree of monodispersity. The mechanisms, however, are not very clear. Monodispersity is best, when the temperature of zone III is kept below the temperature of zone II. Therefore, zone III does not act like the classical LaMER generator's reheater, which revaporizes intermediate condensation products, but instead controls the temperature drop at the end of zone II and thereby the cooling rate of the growing aerosol. The influence of zone III on the structure of the particles will be discussed later.

The flow rate determines the concentration of the NaCl vapours, and therefore influences the size of the aerosol. More important are the effects on the degree of monodispersity which is best at flow rates from o,8 l/min to 1,o l/min. Outside this fairly narrow range the monodispersity decays rapidly. This result is another indication that the degree of monodispersity is controlled by the cooling rate of the growing aerosol.

As already mentioned the number concentrations of the aerosols are very high, and therefore the coagulation processes effect rapid changes of the size distributions. Some very broad size distributions, measured by the ROSL spectrometer after a coagulation time of 2o seconds, are represented in fig. 2o and fig. 21. These size distributions posses a definite structure. Besides the main peak of the single particles several other peaks occur which belong to particles formed by two, three and more NaCl particles. The equivalent sizes of these peaks correspond very well to the equivalent sizes of the doublets, triplets and other aggregated particles in the latex aerosols (21). After dilution at the end of the

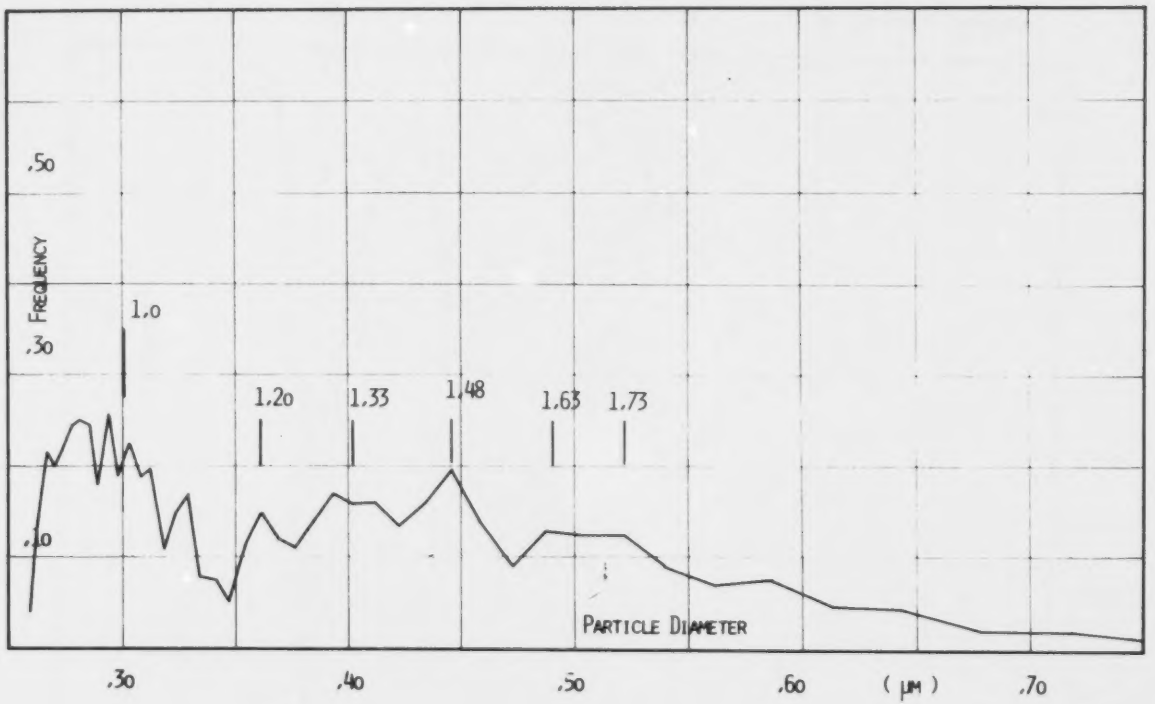

Fig.2o: Number size distribution of heavily coagulated NaCl aerosols. Numbers (1,o ; 1,2 ; etc.) indicate respective multiples of the aerodynamic equivalent diameter of the single spheres in the main peak.

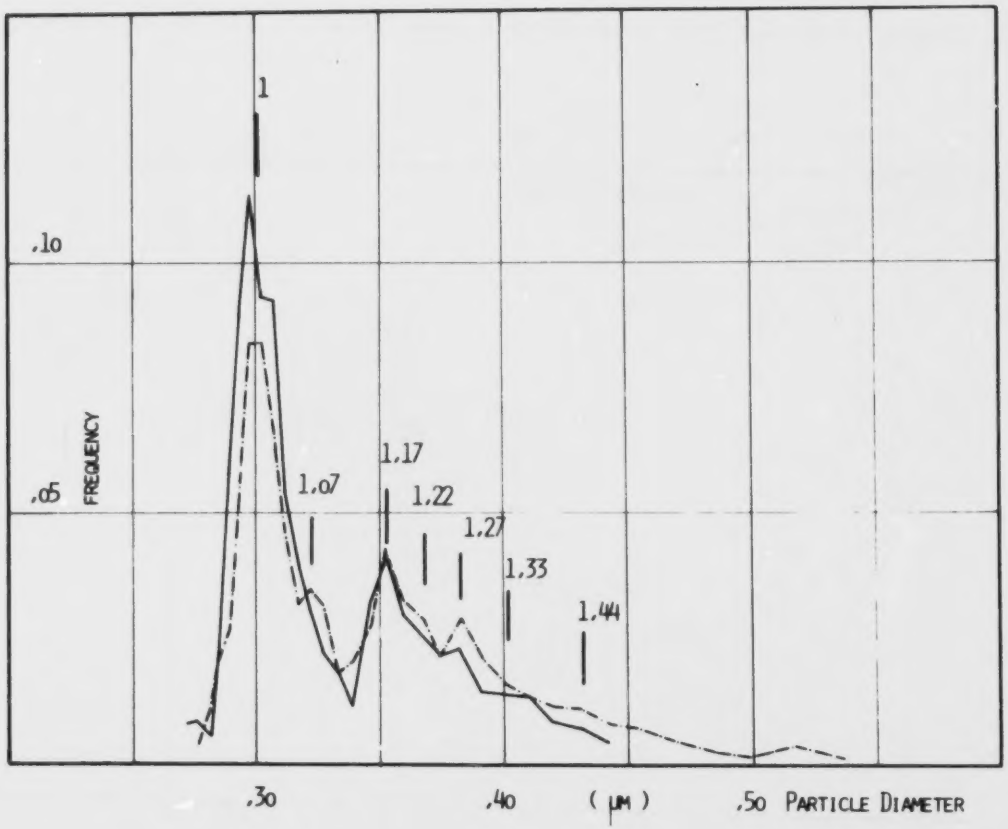

Fig.21: Number size distribution of weakly coagulated NaCl aerosols. Numbers (1,o ; 1,o7 ; 1,17; etc.) indicate respective multiples of the aerodynamic equivalent diameter of the single spheres in the main peak .

center tube, the size distributions are fairly narrow, but still in most of them there occurs a small amount of double particles. The most "pure" of these distributions are logarithmic normal distributions, as shown by the almost straight lines in the log normal plot of the data (fig. 22,23). Deviations at the upper end are due to the double particles.

The density of the particles is a very essential parameter of these aerosols. Deviations from the bulk density which have been reported in the literature (32), would severely restrict the further use of these aerosols, especially with regard to their later application in the diffusion battery experiments, where the centrifuge is used as the reference classifier. The diffusion battery measures a diffusion equivalent size, whereas the size by the centrifuge is a aerodynamic equivalent one. Both sizes are correlated by the density of the particles.

The density of the NaCl particles has been determined by a method described by MATTESON et al (32). The aerodynamic equivalent sizes of the particles are measured by the aerosol centrifuge. The same deposits are analysed by electron microscopy to determine the actual particle diameters at respective deposit locations. Since the aerodynamic size, D_p^*, and the diameter, D_p, are well known, the density is deduced from equ.5

$$\rho_p = (D_p^* / D_p)^{1/2} . B_{pg} \qquad (16)$$

The density derived by this method has been found to be in good agreement with the bulk density of NaCl, and therefore the diameters of the particles can be determined from the aerodynamic equivalent size, D_p^*, by using the bulk density. Diameters measured by the electron microscope and by the centrifuge are in excellent agreement, as shown by fig. 24.(33). It should be mentioned, that the errors, indicated by the bars, and the systematic deviations from the exact relation arise from deficiences in the microscope technique. Moreover the particles are spherical, and the data confirm the assumption that they are perfectly solid and not composed of aggregates of finer particles. The third heating zone seems to favor these properties, because other authors who have produced NaCl

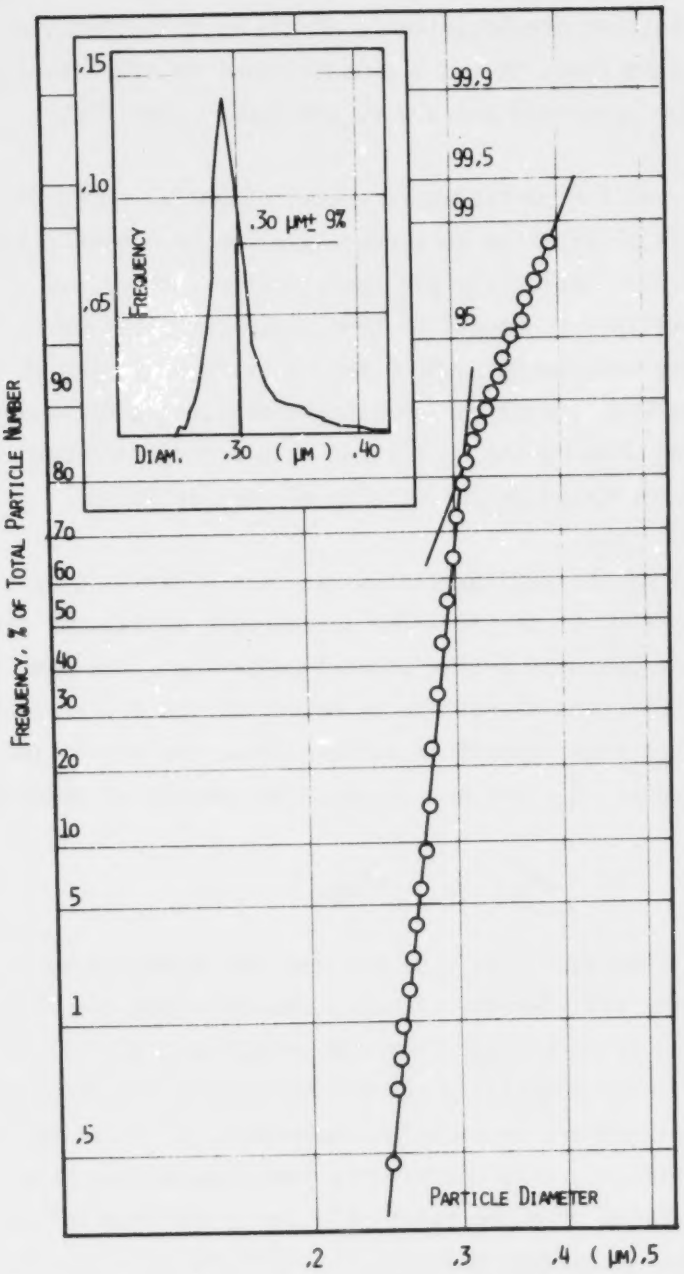

Fig.22 : Number size distribution of diluted NaCl aerosols. Cumulative size distribution (open dots and solid line) and differential size distribution (insert).

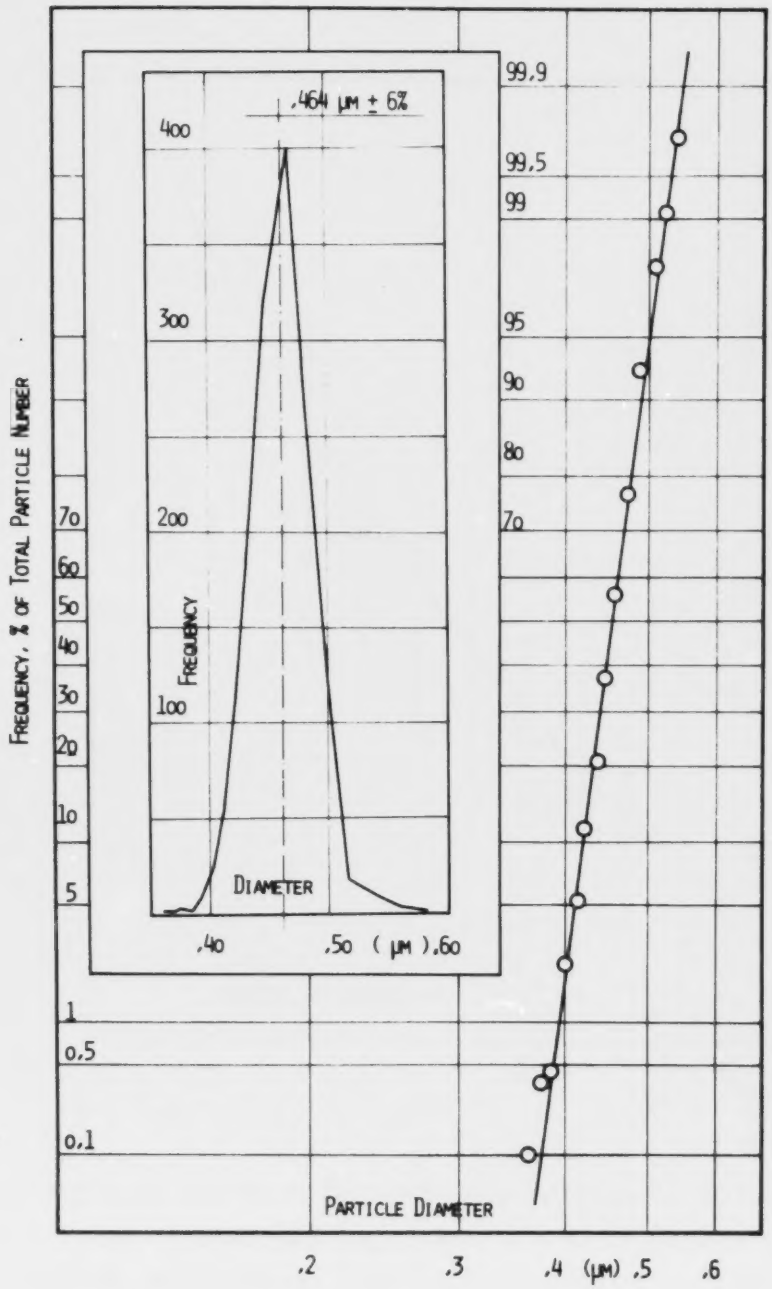

Fig.23: Number size distribution of diluted NaCl aerosols. Cumulative size distribution (open dots and solid line) and differential size distribution (insert).

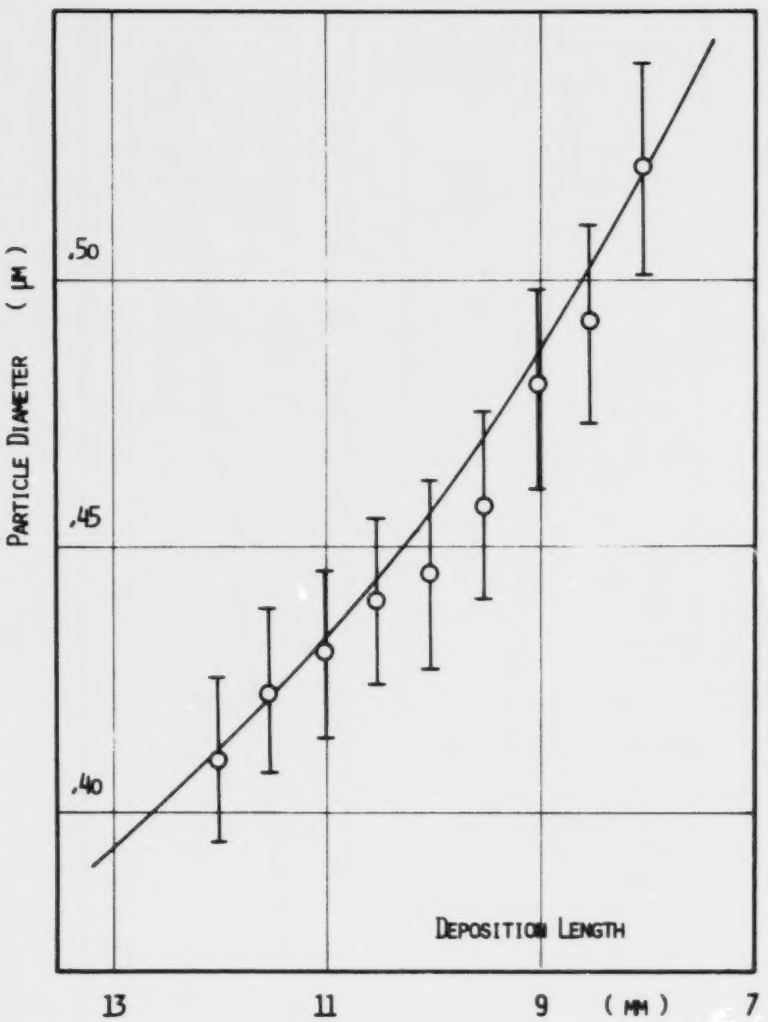

Fig.24: Comparison of electron microscopical diameters of NaCl particles to their deposition lengths in the centrifuge. Experimental data (open dots) and theoretical relationship (solid line) assuming bulk density for the particles.

particles from single heating zone furnaces report surface roughnesses and lower densities ((32), (34), (35)).

The Diffusion Battery

A six stage miniature DB was built using „identical" CHS plates. Its performance was investigated with monodispersed spherical sodium chloride aerosols. Relative standard deviations during the experiments averaged 7 %. The particle concentrations at the exit of the DB were measured by collecting the aerosols on Nuclepore filters and measuring the deposited mass with a flame photometer. The expected mass collection efficiencies were calculated from the DB geometry and the number size distributions of the aerosols and compared with the experimentally determined collection efficiencies. The particle size distributions were measured by the aerosol centrifuge concurrently with each DB experiment.

The experiments were carried out at room temperature and at temperatures between -6^{o} and -75^{o}C. In a previous investigation (28) considerable deviations between experimental and theoretical collection efficiencies at low temperatures were reported. The results described below, obtained with monodispersed spherical aerosols in a water-free, inert carrier gas, do not substantiate the deviations encountered earlier.

The DB (Fig. 25) consists of one prestage (2) and six identical stages (3) (only one is drawn) which are held together by four bolts (5) and are sealed by teflon gaskets. Each stage contains one CHS plate (3b), pressed into position by a steel ring (3a) and sealed by a 0.02 mm gold foil. The CHS plates have diameters of 15 mm and a large number (ca. 4oo ooo) of not quite circular pores with diameters of about 15 µm and lengths of about 5oo µm; porosity is 44 %. The porosity is a very essential parameter for the calculations and has therefore been determined very carefully by four different methods, i.e. (i) from the difference between geometric and true volume by size and weight measurement and known density of the material, (ii) from the difference of weight in air and water, (iii) from determination of open and total surface area by planimetry (from photographs), and

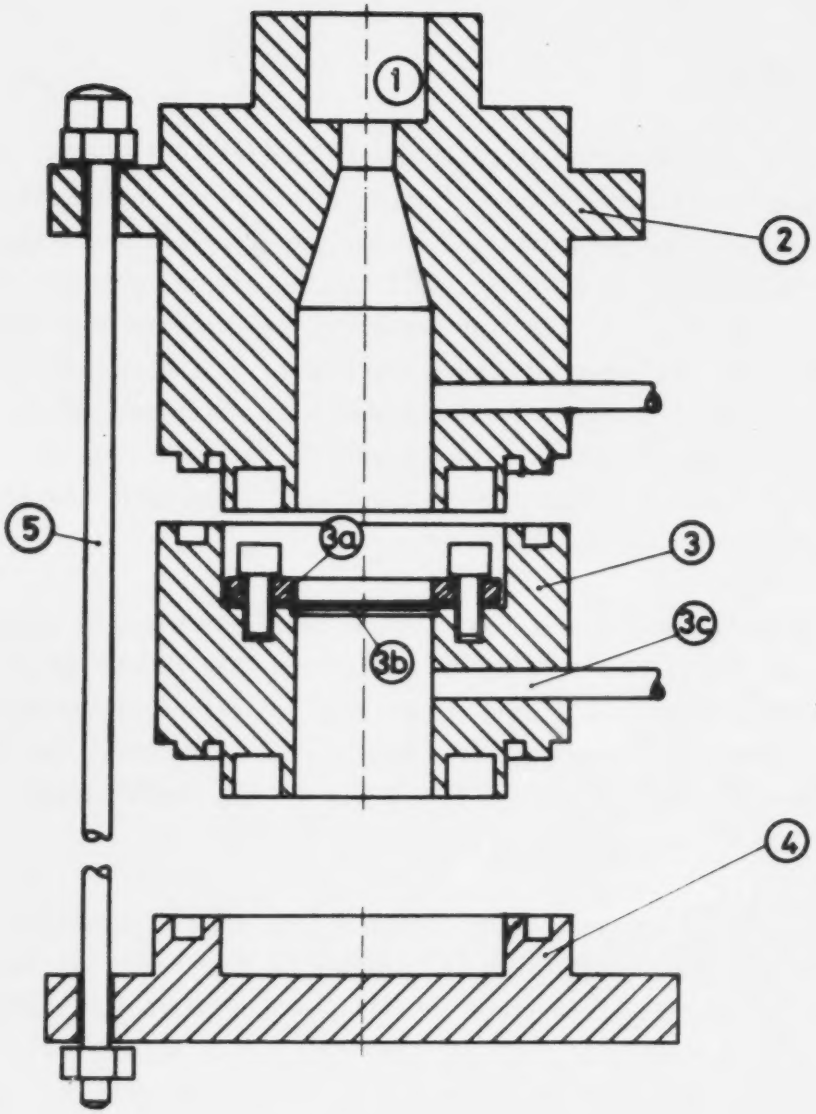

Fig.25: Cross section of the diffusion battery. 1), port into the battery; 2), prestage; 3), diffusion stage with steel ring, 3a), CHS plate,3b), and exit port,3c);4), end plate; 5), clamping bolts.

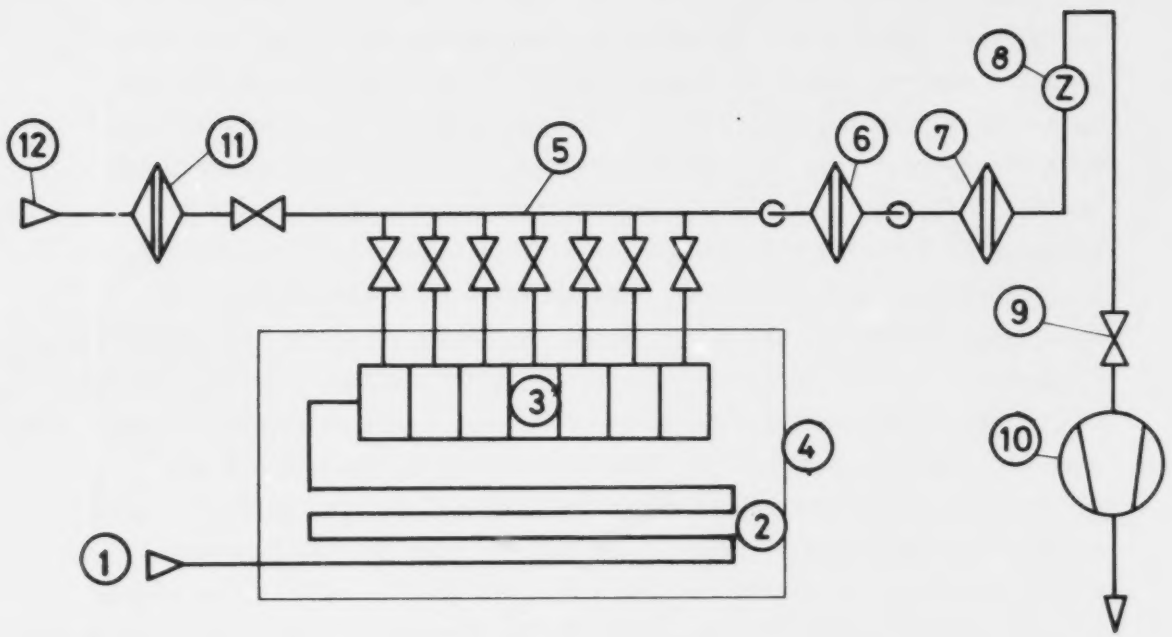

Fig.26: Tubing diagram of the diffusion battery. Aerosol port, 1), and cool-ind coil, 2), in the thermostated bath, 4) ; 3), battery with samplin manifold,5) ; 6) exchangeable filter holder and back up filter, 7) ; 8), flow meter with regulator, 9), and vacuum pump, 1o) ; 12), clean gas port with filter, 11).

(iv) from measured pressure drop versus flow rate across the CHS plates, assuming Hagen-Poiseuille flow. The parameters of different CHS plates vary in a range of about 5 % from the mean. The aerosol flow (fig. 26) enters the DB through a cooling coil (2) (even when no cooling is effectuated to ensure identical conditions for all experiments). At the inlet of the DB the temperature is monitored with a thermocouple.

Each stage of the DB has an exit tube of 3 mm inner diameter with a stainless steel valve. By switching the appropriate valves the aerosol passes a desired number of stages (3) and is then led through the exit tube into a sampling manifold (5). The manifold is immediately followed by a nuclepore filter (6), which serves as the concentration measuring device. Though a specially designed filterholder (35) permits quick exchange of filters, this procedure still is slower than reading e.g. a condensation nucleus counter. Nevertheless the filtration method was chosen because of the difficulties in compensating for the pulsations in aerosol flow introduced by most condensation nucleus counters. Tubing can be held very short and particle losses are minimized; in addition care is taken to avoid high particle velocities or sharp bends and eddies with subsequent impaction in the flow system. The particle concentrations are measured alternately at the prestage and behind the selected number of stages of the DB. Between measurements the manifold is always flushed with filtered clean gas through an additional inlet. For experiments at low temperatures the DB is immersed in a cold bath, consisting either of a mixture of NaCl and ice (to - 2o^{o}C) or of dry ice - acetone (to -75^{o}C). All gas streams entering the DB are dried with $Mg(ClO_4)_2$ and P_2O_5. (If the aerosol is not dried sufficiently, water vapour condenses on the CHS plates and freezes in their pores). Glass tubing is used exclusively.

Deposition mechanisms in a diffusion battery

The theory of deposition in flow systems has been investigated extensively; only the relevant expressions will therefore be reviewed briefly. Particle deposition takes place by impaction and interception on the face of a CHS plate and by diffusion and sedimentation in its channels.

An estimation of the effects of electrical deposition by image forces and of sedimentation in the presence of diffusion (37), (38), (39), shows that both may be neglected. So only diffusion, impaction and interception will be considered.

Diffusion

The semiempirical expression given by THOMAS (4o) was chosen as most convenient for diffusional deposition in circular channels at Poiseuille flow because it covers the whole studied range of the diffusion parameter μ, which is given by

$$\mu = \pi \frac{D.l.n}{Q} \tag{17}$$

D ..... diffusion coefficient
l ..... channel length (plate thickness)
n ..... number of parallel channels
Q ..... volume flow rate

THOMAS gives the following expression for the diffusional deposition efficiency:

$$E_D = 1 - \{0.819 \exp(3.657\mu) + 0.097 \exp(-22.3\mu) + 0.032 \exp(-57\mu) + 0.027 \exp(-123\mu) + 0.025 \exp(-750\mu)\} \tag{18}$$

Results obtained from the analogue expressions of TWOMEY (41) differ only by less than 0.1 % from the values of THOMAS (4o) in the range of μ from 0.001 to 0.05.

Impaction

A simple model of particle flow to the surface of filters was studied

by PICH (42). He gives the following expression for the impaction efficiency E_i:

$$E_i = \frac{2\,z}{1+G} + \frac{z^2}{(1+G)^2}$$

$$G = \frac{\sqrt{P}}{1 - \sqrt{P}}$$

$$z = 2\ St.\ \sqrt{G} + 2\ St^2.G(\exp\{1/St.\sqrt{G}\}-1) \qquad (19)$$

with

P ..... porosity
St .... Stokes number

SMITH and PHILLIPS (43) found values for inertial collection by solving the differential equations of flow with a computer. Their model is probably closer to reality and also accounts for finite particle size, but the lack of analytical expressions makes its application difficult, so it is not used.

Interception

A formula governing interception efficiency E_R is given by SPURNY (44). It can be derived from simple geometric considerations and may be applied to CHS plates treating them like Nuclepore filters in first approximation

$$E_R = N_R\ (2 - N_R) \qquad (2o)$$

where N_R is the ratio of particle to pore diameter.

SMUTEK and PICH (45) studied a more complicated model of flow which leads to rather complex expressions, giving a combined impaction and interception efficiency as well as an impaction efficiency alone; in the following they will be refered to as E_{iR}' and E_i'.

Combinations of Deposition Mechanisms

Deposition by diffusion, impaction and interception occurs simultaneously, so expressions have to be derived for the combination of these processes. One possible way is to assume their independence. Total penetration through the system (e.g. a filter, a CHS plate) is then found by multiplication of the partial penetrations. Hence the combined penetration for diffusion and impaction, T_{Di}, is

$$T_{Di} = T_D . T_i \tag{21}$$

and for additional interception it is

$$T_{DiR} = T_D . T_i . T_R \quad ; \tag{22}$$

the respective collection efficiencies are

$$E_{Di} = 1 - T_{Di} = E_D + E_i - E_D . E_i \tag{23}$$

and

$$E_{DiR} = 1 - T_{DiR}, \tag{24}$$

the use of either T or E is a question of convenience.

Equ. (21) is accepted by several authors for filter deposition (39), (44), (46), (47), generally in the form of equ. (23). It has also been used to correct DB data for impaction (28). The combined deposition efficiency of all three mechanisms, however, does not seem to be given correctly by equ. (22). Semiempirical formula have been used instead, which are derived from equ. (24) by introducing weight factors for interception (46), (47). These factors are determined from experiments and reduce the relative influence of interception considerably. A theoretical explanation has not yet been given and the fact that no filter material is perfectly regular introduces additional problems.

The expression which was used here is

$$E_{DiR} = E_i + (1-E_i)\,(E_D + E_R\, 0.63^{(1-N_R)}) \qquad (25)$$

with the same numerical constants as used by SPURNY et al. (47). Another possible formula for combined penetration is derived from equ. (22) by using the SMUTEK-PICH expression for impaction and interception, E_{iR}', instead of equ. (19) and (2o). Combined penetration then reads

$$T_{DiR} = T_D \cdot (1 - E_{iR}') \qquad (26)$$

It is interesting to note that the values computed for impaction efficiencies from the SMUTEK-PICH expression are negligibly small compared to those from equ. (19) in the range of particle sizes and velocities studied. The values from the SMUTEK-PICH expression represent practically only interception as can be seen from fig. 27 showing computed curves for combined impaction and interception efficiences. The flow rate is chosen as parameter and increases from 0.2 to 1 l/min in steps of 0.2 l/min which represents the typical range of experimental values. For curves 1 to 5, equ. (25) for E_{DiR} was used, setting $E_D = 0$. Efficiency increases markedly with flow rate by increased impaction while interception remains constant. For the same variation of flow rates the efficiency curves from the SMUTEK-PICH formula, E_{iR}', coincide practically (curve 6 for o.2 l/min and curve 7 for 1 l/min) because the contribution from impaction is very small.

The above discussion shows the difficulties in selecting appropriate expressions for deposition from impaction and interception purely from theoretical considerations - in contrast to diffusional deposition where numerical results calculated from several authors are nearly identical. Values derived from different impaction and interception formulas and their combinations were therefore directly compared to experimental data.

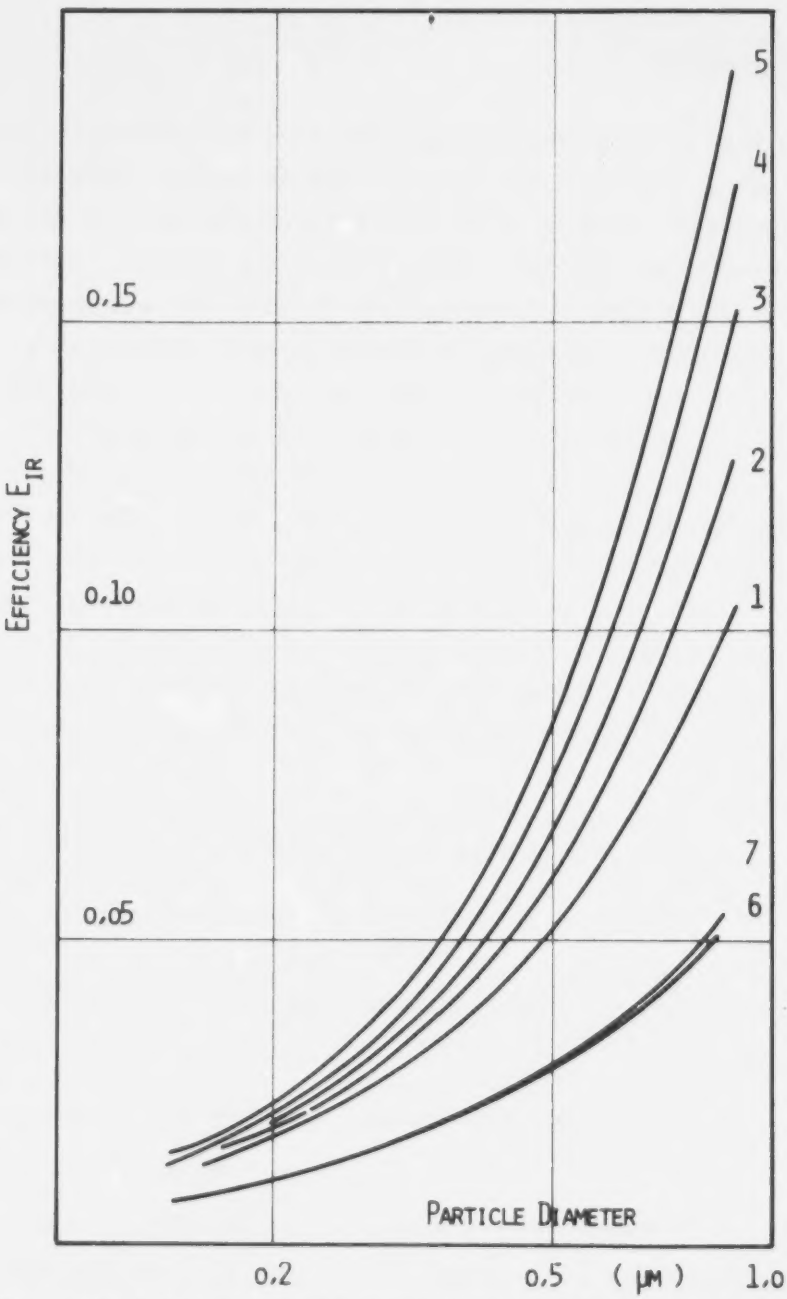

Fig.27:Theoretical impaction and interception efficiency of CHS plates at different flow rates. Curve 1 to curve 5, efficiencies increasing from o,2 l/min to 1 l/min. Curves 6 and 7, theoretical expression with underestimation of impaction.

Results and Discussion

The main goal of this work is the comparison of theoretical and experimental values for diffusion coefficients at various temperatures. For this purpose the diffusion deposition efficiencies must be derived with high accuracy from the total deposition in the DB. Contributions of different particle deposition mechanisms to total deposition were therefore investigated. Sedimentation proved to be negligible under the experimental conditions given, so, in addition to diffusion, only impaction and interception were considered. The results of 13 experiments are presented in Table 2. Four parameters are given in columns 1 to 4 characterising each experiment: mean geometric particle diameter and relative standard deviation measured with an aerosol centrifuge, aerosol flow rate and temperature. Columns 5 and 6 contain the measured penetration, T_{exp}, per stage averaged over all 6 stages of the DB, and its relative standard deviation σ_{rel}. The calculated penetration values are listed in columns 7 to 12 for the following set of mechanisms and their combinations:

T_D, T_i, R_R	for diffusion, impaction and interception, respectively, from formulae (18), (19) and (2o).
T_{Di}	combination of diffusion and impaction by formula (21)
T_{DiR}	combination of diffusion, impaction and interception by formula (25)
$T_D \cdot T_{iR}'$	combination of diffusion, impaction and interception by formula (26)

Values are always calculated for a diffusion length of one stage, with parameters averaged over all 6 stages. Other possible combinations with T_R, as $T_D \cdot T_R$ or $T_D \cdot T_i \cdot T_R$, have been omitted because their values were too far off from T_{exp} according to our measurements.

For better correspondence between computed penetration and experimental values, T_{exp}, the penetrating mass for each fraction of the aerosol number

TABLE 2. EXPERIMENTAL AND THEORETICAL TRANSMISSIONS OF THE DIFFUSION BATTERY

1) D_p	2) s_{rel}	3) Q	4) Temp.	5) T_{exp}	6) s_{rel}	7) T_D	8) T_i	9) T_R	10) T_{Di}	11) T_{DiR}	12) $T_D T_{iR}$
o,452	18,4	o,19	25	o,84o	1,5	o,864	o,991	o,932	o,857	o,813	o,844
o,334	12,5	o,31	25	o,847	2,5	o,868	o,993	o,952	o,862	o,832	o,835
o,238	8,9	o,39	25	o,827	2o,o	o,845	o,996	o,966	o,841	o,82o	o,8o5
o,3o6	17,5	o,38	- 6,1	o,865	2,5	o,875	o,992	o,954	o,868	o,839	o,837
o,594	5,8	o,85	-19,6	o,885	1,o	o,955	o,942	o,918	o,9oo	o,85o	o,86o
o,489	5,7	o,5o	25	o,894	5,o	o,926	o,979	o,932	o,9o7	o,864	o,87o
o,52o	8,9	o,5o	25	o,887	3,6	o,93o	o,976	o,927	o,9o7	o,861	o,874
o,52o	8,9	o,5o	25	o,887	3,6	o,93o	o,976	o,927	o,9o7	o,861	o,874
o,417	5,o	o,41	-2o,6	o,876	1,5	o,9o8	o,985	o,942	o,896	o,858	o,863
o,439	4,2	o,32	-73,2	o,871	2,1	o,899	o,985	o,94o	o,885	o,847	o,864
o,493	5,2	o,67	-68,5	o,9o3	3,o	o,941	o,962	o,932	o,9o5	o,863	o,866
o,5o5	5,6	o,65	-75,4	o,884	3,4	o,941	o,96o	o,93o	o,9o4	o,861	o,869
o,594	11,o	o,5o	25	o,894	o,5	o,937	o,967	o,916	o,9o6	o,854	o,879
o,568	8,7	o,6o	- 7,2	o,886	2,4	o,937	o,967	o,921	o,9o5	o,856	o,871

1) D_p, particle diameter (µm); 2),6): s_{rel}, relative standard deviation (± %); 3) Q, flow rate (l/min); 4) temp, temperature at the diffusion battery (^oC); 5) T_{exp}, experimental transmission of the battery, 7)-12) T_{ij}, theoretical transmissions, calculated by using the experimental values from 1) - 4).

distribution was calculated independently. Total penetration was then obtained by adding the single fractions and dividing by the whole incoming mass of aerosol.

In Table 3 the relative differences in percent between T_{exp} and theoretically predicted penetrations are listed using the same set of combinations as in Table 1 and additionally $T_D \cdot T_R$ and $T_D \cdot T_i \cdot T_R$. The mean values given below each column can be interpreted as systematic deviations and thus indicate whether the respective theoretical expressions tend to give higher of lower values than total experimental deposition. Diffusion alone (column 1) obviously leads to a value of T which is markedly higher than T_{exp} (+ 4 %); diffusion together with impaction (column 2) gives the closest fit to the experiment (+ 1,6 %) when equ.(21) is used for impaction. Column 2 with an average difference of 3 % between theory and experiment shows clearly, that interception is overestimated by equ. (2o), as already mentioned above. The values in columns 4 to 6 comprise all three mechanisms. Simple combination of these mechanisms by multiplication (column 4) gives penetration values that are markedly lower than the experimental ones (- 5 %). The probable reason again is an overestimation of interception. The average deviation for the semiempirical equ. (25) from SPURNY (47) in column 5 is about the same as for the combined impaction-interception equ. (26) from SMUTEK-PICH (column 6). It is somewhat higher than that for T_{Di} in column 2, but still lies within the error margins of about 3 % for our DB experiments. In Fig. 28, finally, the above results are displayed graphically for one selected DB experiment. Values of T_{exp} for increasing numbers of DB stages (dashed line) are drawn together with the error limits of the measured penetration. The other curves correspond to the above set of computed values for T. It is interesting to compare the values of diffusion coefficients D and particle diameters D_p from DB measurements to those from the aerosol centrifuge. Considering that the relative deviation of T_{exp} from T_{Di}, averaged over all data, was only 1,6 % (table 3) with constant tendency in the same direction (such an error is insignificant for a DB measurement !), it was at first surprising to find that experimental and theoretical values of D and D_p differ by about 1o %. It may be recalled here, that this is a purely

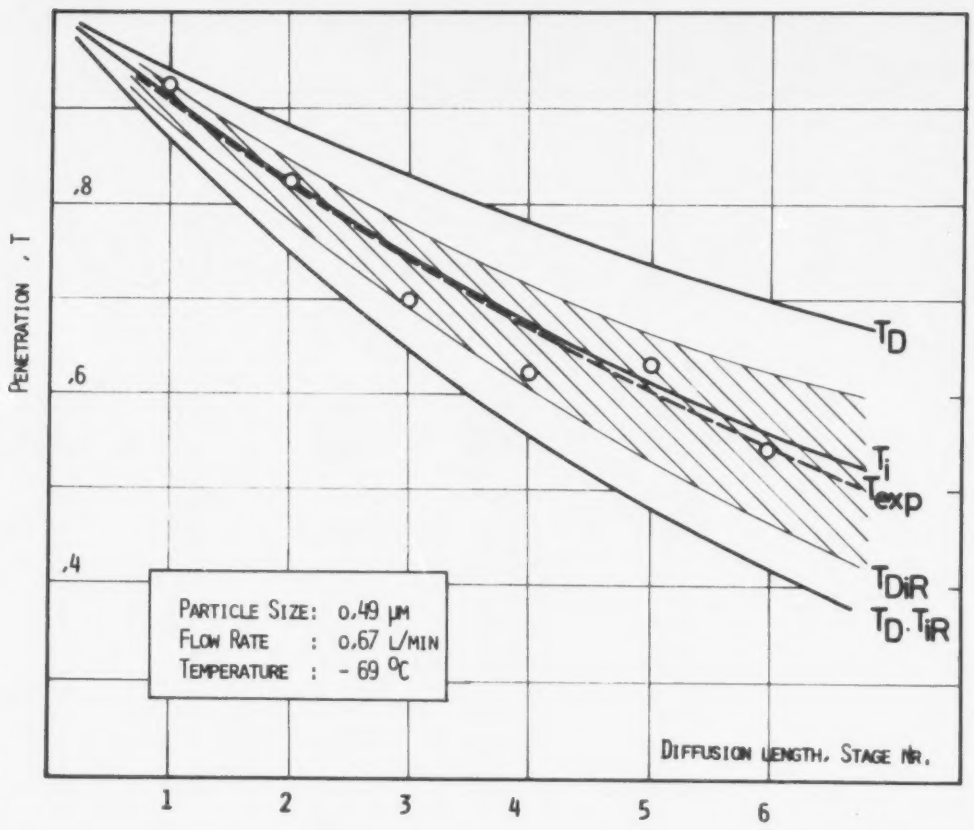

Fig.28: experimental transmission data compared to theoretical expectations. The shaded field illustrates the region of experimental confidence.

TABLE 3. DEVIATIONS OF THEORETICAL TRANSMISSIONS FROM EXPERIMENTAL VALUES. T(experim) = 1oo %

1) T_D	2) T_{Di}	3) T_{DR}	4) $T_D T_i T_R$	5) T_{DiR}	6) $T_D T_{iR'}$
2,9	1,9	-4,2	-5,o	-3,2	-o,5
2,5	1,8	-2,4	-1,8	-3,1	-1,5
2,2	1,7	-1,3	-1,7	-o,8	-2,7
1,2	o,3	-3,5	-4,3	-3,o	-3,2
7,9	1,7	-o,9	-6,7	-4,o	-2,8
3,5	1,4	-3,8	-5,8	-3,7	-3,o
4,8	2,3	-2,8	-5,1	-2,9	-1,5
3,7	2,2	-2,4	-3,8	-2,1	-1,5
3,2	1,6	-3,o	-4,4	-2,8	-o,8
4,2	o,2	-6,4	-1o,o	-4,4	-4,1
6,2	2,2	-1,2	- 5,2	-2,8	-1,9
4,8	1,3	-4,o	- 7,2	-4,5	-1,7
5,8	2,1	-2,6	- 4,9	-3,4	-1,7
4,o	1,6	-2,9	- 5,o	-3,1	-2,1

numerical consequence of the evaluation method: The value of T_{exp} is at first corrected for impaction by dividing by T_i; then the transcendental equ. (18) is solved for μ from which D and D_p are finally obtained. As T depends exponentially on μ , errors in D cannot be simply calculated from the relative error in T, they also depend on the absolute value of T. For this reason T was used to study deposition in our DB and not D or D_p.

As already mentioned above, the DB was also tested at lower than ambient temperatures, between -6^{o} and $-75^{o}C$, with spherical sodium chloride particles in a stream of carefully dried nitrogen. Results do not differ significantly from the measurements at room temperature listed in Tables 2 and 3. It should nevertheless be mentioned here, that deviations were observed in a few early experiments; these were in the same direction and order of magnitude as earlier reported data (28). It seems, though, after studying possible correlations to other effects that most probably the cold bath surrounding the DB was not sufficiently homogeneous in temperature and so thermal diffusion could have taken place. The additional deposition effect was about 5.5 %. One suche experiment at $-74,5^{o}C$, e.g., gave a penetration T_{exp} which was about 7 % below the theoretical value T_{Di} listed in column 1o of table 1. This led to a diffusion coefficient of $1.9 \times 1o^{-6}$ cgs units instead of $o.63 \times 1o^{-6}$ - the difference is 2oo %. In subsequent experiments care was taken to avoid this source of error and good agreement was obtained afterwards.

THE FIVE STAGE LOW PRESSURE IMPACTOR

Introduction

Cascade impactors are used for the determination of size distributions of airborne particulate matter. In the impactor the aerosol is precipitated on a series of stages, where each stage collects a certain size category of the aerosol. Cascade impactors have been developed in many different designs, mainly for application to special purposes. A stimulating goal for further developments of cascade impactors is the determination of the mass size distributions of urban aerosols in correlation with their chemical composition.

A five stage cascade impactor for mass analysis is represented in fig. 29. The aerosol enters the instrument by a ring slit between the top cover and the cylindrical housing. This slit and the inner side of the cover constitute the entrance stage, i.e. stage 5, which has a cut off point of 25 µm. Particles of larger sizes are deposited on a thick layer of vaseline in order to prevent blow off and bouncing. The rest of the aerosol passes to the next stage which collects all particles larger than 6,4 µm. This stage, i.e. stage 4, consists of a circular orifice plate with a set of identical holes with sharp, rectangular edges, and of an impaction plate with a large center hole for the flow.Distance between these plates is made by a ring at the periphery of the stage. This arrangement is repeated in each of the following stages. The cut off points of these stages are 1,6 µm for stage 3; o,4 µm for stage 2; and o,1 µm for stage 1. The volume flow rate is 8o l/min at standard

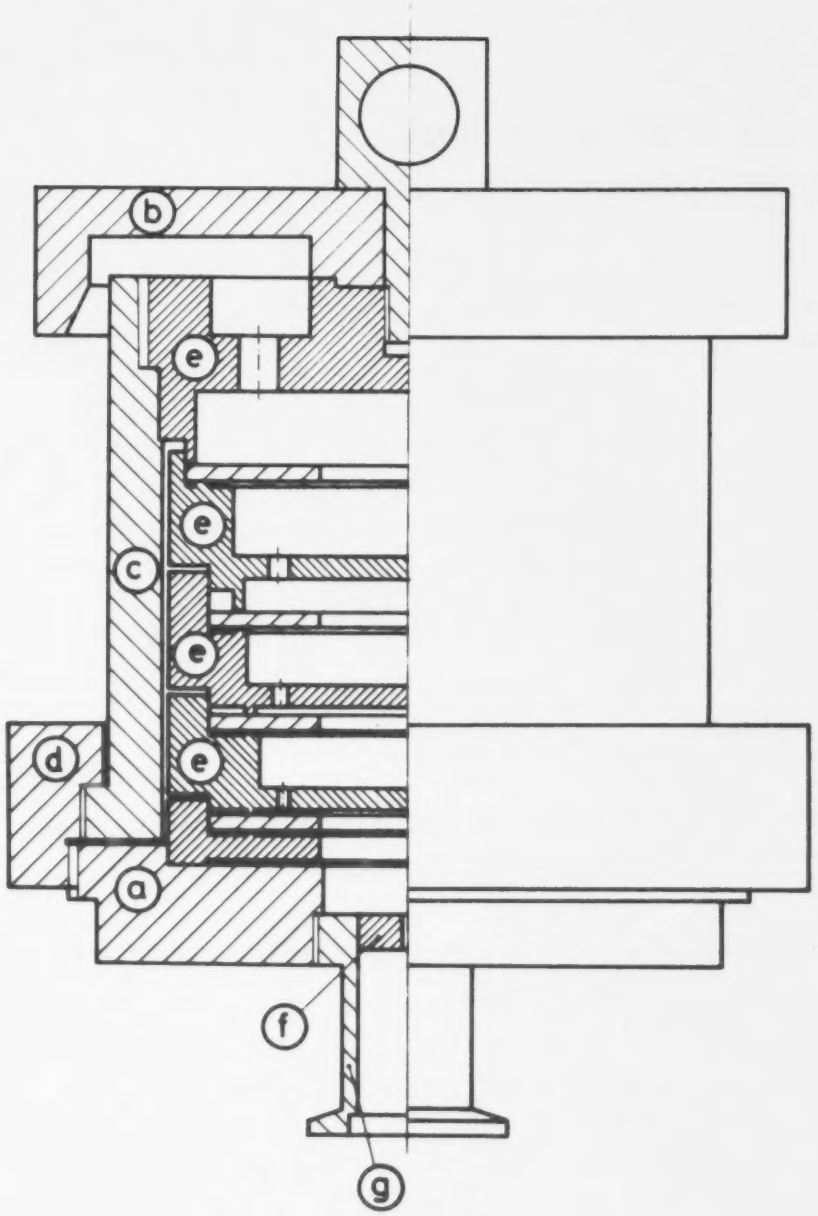

Fig.29: Cross section of the five stage low pressure impactor. A, base plate with critical orifice,F, and vacuum pump adapter, G; parts of the housing: B, cover; C, mantle ; D, nut ; E, impaction stages.

TABLE 4. DATA OF THE IMPACTOR STAGES

1)	2) D_p^x	3) W	S	L	N	4) p_i/p_o	p_a/p_o
4	6,25	o,55	1,2o	1,1o	11	1,oo	1,oo
3	1,58	o,17	o,6o	o,5o	24	1,oo	o,996
2	o,38	o,o7	o,2o	o,2o	33	o,996	o,859
1	o,1o	o,o5	o,15	o,15	2o	o,859	o,335

1) stage number

2) cut off diameter (μm)

3) W, orifice diameter (cm); S orifice-to-plate distance; (cm); L, orifice length (cm); N, orifice number

4) p_o, atmospheric pressure; p_i, pressure ahead of the orifices; p_a, pressure below the orifices.

temperature and pressure. The flow is controlled by a critical orifice in the base plate of the impactor. Other data on this impactor are listed in table 4.

Each orifice plate has a number of identical orifices which are placed on a circle, concentric to the axis of the stage. This arrangement effects an equal flow partition, and consequently the aerosol deposits are equally partitioned during sampling. For sufficiently large distances between the orifices, the deposits are localized in a number of separated spots. Investigations have shown that these spots carry equal amounts of the total deposit.

The impaction plate is covered by a foil. This feature is advantageous for weight analysis because the foils can be cut from very thin material to keep their weight at a low level and because the selection of foil materials can vary according to the needs of the analysis. Aluminum foils of 10 μm thickness have been used successfully for measuring mass size distributions of solid and semi-liquid particles, and foils of filter membranes such as millipore cellulose membranes are very convenient for the collection of liquid materials like oil.

A certain amount of the material is deposited on other surfaces of the stages. These wall deposits are of significance, because they limit the practical use of the impactor. In many cases there is no possibility or justification to determine these deposits separately in order to include them into the results. Therefore they should preferably be negligibly small. The impactor described here has wall deposits the order of a few percent of the total deposits of a stage, an amount which may be neglected in practice. The wall deposits, however, increase when the total load of a stage is raised beyond certain limits.

Particle size analysis

An impactor stage is composed of an orifice plate and of an impaction plate, which are separated by a distance S. The orifice plate has circular

orifices of diameter W. The orifices have the length L.

The aerosol is drawn through the orifices by means of a vacuum pump. Aerosol jets are produced, which are deflected by the impaction plate. For sufficiently large orifice distances, S > W, the flow has three sections, i.e. the free jet flow ahead of the impaction plate, the stagnation flow at the impaction plate near the stagnation point, and the free wall jet at the impaction plate outside the region of stagnation. For sufficiently long orifices, L > 2W, and for moderate pressure drops along the orifice, the free jet has the diameter, W, and its velocity is identical to the gas velocity, u_o, in the orifice. The wall jet has similar characteristics. The velocity is again u_o, if friction losses are neglected, and the jet flows in a layer of thickness, $H_o = (1/8).W$, approximately. (48).

In the region of stagnation the gas velocities undergo changes with respect to amount and direction, and relative velocities between the particles and the gas occur. The particles change their velocities according to the STOKES law, which is given by

$$\dot{\vec{v}} = -(3.\pi.\eta_g.D_p/m_p.B_{pg}).(\vec{v} - \vec{u}) \qquad (29)$$

where $\vec{v}$ is the velocity of the particle, $\vec{u}$ the velocity of the gas at the particle's position, and m_p the mass of the particle. The slip correction factor, B_{pg}, depends on the KNUDSEN number, $K = 2.\lambda_g/D_p$, according to equ. (3o)

$$B_{pg} = (1 + K.(1,257 + o,4 \exp(-1,1.K^{-1})) \qquad (3o)$$

where λ_g is the mean free path of the gas molecules which equates to

$$\lambda_g = 1o,8 \cdot (\eta_g/P) \cdot (T/M)^{1/2} \qquad (31)$$

where the gas has the temperature, T, the pressure, P, and the molecular weight, M. It should be noted that T and P are the values of temperature and pressure at the location of the particle.

By introducing the relaxation time, τ_p, of the particle

$$\tau_p = (1/18).(D_p^2.\rho_p.B_{pg}).(1/\eta_g) \qquad (32)$$

the equation of motion (29) becomes

$$\dot{\vec{v}}/(\vec{v}-\vec{u}) = -(1/\tau_p) \qquad (33)$$

which shows very clearly the significance of the relaxation time. Changes of the particle velocities are inversely proportional to the relaxation time, with regard to comparable relative velocities. Consequently, in the region of stagnation the trajectories of particles with large relaxation times are almost undisturbed continuations of the trajectories in the free jet. These trajectories will end on the impaction plate. Sufficiently small particles follow almost perfectly the streamlines of the gas, and therefore their trajectories do not end on the impaction plate.

The separation curve $T(\tau_p)$ is a very convenient means to describe the efficiency of the stage. $T(\tau_p)$ is zero for sufficiently small particles, and its numerical value is one for large particles. In an intermediate range of relaxation times, $\Delta\tau_p$, the separation curve increases from T = 0 to T = 1 monotonously, at ideal conditions. In the range $\Delta\tau_p$ the separation curve assumes the value $T(\tau_o)$ = o,5 for a certain relaxation time, τ_o, i.e. the critical relaxation time. This time is determined by calculation or experimentally. The approximate numerical value for the critical relaxation time is estimated by considering the particle flow in the region of stagnation. All of the deposited particles, at least those with relaxation times near the critical time, enter the region of stagnation with the velocity, u_o, of the jet. Their path from the periphery of the region of stagnation down to the plate, vertically, is of the order of the wall jet thickness, H_o. The smallest particles that contact the plate do so with almost zero velocity (vertically to the plate) and arrive after a time of the order

$$\tau' = H_o/u_o = (1/8).(W/u_o) \qquad (34)$$

This time is approximately the critical relaxation time, τ_o, for round jets. According to equ. (34), the critical relaxation time is independent of the physical constants of the particles and of the gas, but depends on the jet velocity and the jet diameter, and therefore characterizes the stage properties.

Deposition of a particle occurs when its relaxation time is larger than the critical relaxation time, and particles are not deposited when their relaxation time is smaller. Thus, the relative relaxation time, ϕ , of a particle is decisive for deposition,

$$\phi = \tau_p/\tau_o = (4/9).(D_p^2.\rho_p.B_{pg}/\eta_g).(u_o/W) \qquad (35)$$

In accordance with this equation the collection efficiency curve is often represented by $T(\phi)$. Other equivalent parameters, which differ from ϕ by factors only, are the STOKES number and the inertial parameter. Other properties of the collection efficiency curve should be mentioned. Efficiency curves of different, but geometrically similar stages unite quite well in one curve, if certain conditions are observed, e.g. the REYNOLDS number $R_e = (W.u_o.\rho_g/\eta_g)$ of the orifice flow should fall into the range 3oo < Re < 6ooo. In this case the averaged separation curve $\overline{T}(\phi)$ assumes the value $\overline{T}(\phi)$ = o,5 at ϕ_o = o,88. In the intermediate range, which is for most impactors less than $\Delta\phi$ = o,3.ϕ_o, the collection efficiency curve increases monotonically, and may be influenced by the surface structure of the impaction plate or by flow turublences. However, the exact shape of the curve in this region is not very significant for the performance of a cascade impactor.

The aerodynamic equivalent size

In the stagnation flow different particles can exhibit trajectories which are identical point for point in laminar flow, or which coincide on an average curve in turbulent flow. Regarding the points or short elements of such a trajectory, one may state that it is correlated to a definite relaxation time. Consequently, all particles on such a path have identical

relaxation times, and can not be discriminated aerodynamically, i.e. by observation of different paths.

The particle category, which belongs to a definite relaxation time, τ_p, does not only contain spherical particles, but also particles of many other regular and irregular shapes. The spheres within this category possess the relaxation time $\tau_p = (D_p^2.\rho_p.B_{pg})/(18.\eta_g)$, and among them is the sphere with the density $\rho_p = \rho_e = 1$ and with the diameter, D_e,

$$D_e = ((\tau_p.18.\eta_g)/(\rho_e.B_{eg}))^{1/2} \qquad (36)$$

This diameter is the aerodynamic equivalent size for the particle category under consideration.

For a certain relaxation time, the equivalent size can not be deduced from equ. (36), because the slip correction factor is unknown. But this equations leads immediately to

$$D_e^2 \,.\, B_{eg} = (\tau_p.18.\eta_g)/(\rho_e) \qquad (37)$$

which divided by $4.\lambda_g^2$ and combined with equ. (3o) yields

$$K_e^{-2} + K_e^{-1}\,(1,527 + o,4.\exp(-1,1.K_e^{-1})) = (\tau_p.18.\eta_g)/(4\lambda_g^2.\rho_e) \qquad (38)$$

where the mean free path of the gas molecules follows equ.(31). In equ.(38), the numerical value of the KNUDSEN number K_e is found by iteration, and finally the equivalent diameter is calculated from this KNUDSEN number.

The equivalent cut off diameter, D_o, of an impactor stage is defined by introducing $\tau_p = \phi_o.\tau_o = o,88.\tau_o$ into equ. (36)

$$D_o = ((o,88.18.\eta_g.W)/(8.u_o.\rho_e.B_{eg}))^{1/2} \qquad (39)$$

and is calculated by using equ. (38) for the KNUDSEN number K_o.

Impactors are often tested with spherical particles with densities different from $\rho_e = 1$. For identical relaxation times the relation $D_e^2 \cdot \rho_e \cdot B_{eg}(\lambda_g, D_e) = D_p^2 \cdot \rho_p \cdot B_{pg}(\lambda_g, D_p)$ is valid for these particles and their equivalent size is defined by

$$D_e = D_p \cdot (((\rho_p \cdot B_{pg}(\lambda_g, D_p))/\rho_e \cdot B_{eg}(\lambda_g, D_e))^{1/2} \qquad (4o)$$

In this formula the brackets accompanying the slip correction factors indicate their dependence on the mean free path and of the particle diameters. In consequence, the equivalent size of a given particle with diameter, D_p, and density, ρ_p, will vary for different mean free paths, λ_g. However, the variations are small for common aerosols.

Deposits in the impactor stages

The main deposits, which occur immediately beneath the orifices, are round spots with a diameter of 1,2 times to 1,7 times the orifice diameter. These spots are clearly isolated when the interorifice distances are large enough, and for this reason values of four times to seven times the orifice diameter have been chosen. Beside the spots other deposits occur. Halos surrounding the spots are found which at low loads are clearly separated from the spots by an almost particle - free zone. The mechanisms of halo formation are still controversial, but it has been proposed that turbulence in its very beginnings is responsible for this deposition (49). Deposits occur between the spots along a narrow straight line, in radial direction with respect to the axis of the stage. This is a very interesting phenomenon, because the line appears at the confluence of two wall jets from adjacent orifices. In this region the wall jets detach from the impaction plate forming a new, upward flowing jet. The existence of this jet is indicated by straight deposit lines on the upper plate in between the orifices. The deflection of the wall jets requires a stagnation flow in the region of confluence, and consequently the deposit line marks the stagnation line. Moreover, turbulence along this line is indicated, because particles would not be deposited otherwise. The amount of material in the halos and in the

stagnation lines is in most cases a few percent of the mass in the spots. Therefore these deposits do not affect the results seriously when they are integrated into the measurement, i.e. by weighing the samples.

Other deposits occur on the inner wall of the ring spacers where the wall jets hit, and at the underside of the orifice plate as already mentioned above, and predominantly around the mouth of the orifices on top of the orifice plate. These wall deposits limit the practical usefulness of the impactor because they are usually not easily included in the measurements, and therefore they should preferably be small. The wall deposits of the impactor have been determined by using vaseline aerosols, produced by spraying from a heated nebulizer and containing a soluble dye, i.e. sudan red, as a tracer. This mixture disolves readily in toluene, and consequently the amount of dye as well as the deposited aerosol mass can be determined by absorption photometry. In addition, this aerosol permits the control of the weight analysis by photometry.

As shown by the graphs in fig. 3o, stage 2 and stage 3 have wall losses of 3 % to 4 % of the total mass deposited in the stages for moderate loads of a few milligrams per stage. For higher loads the amount of wall deposit increases. One possible explanation for this behaviour is based on the assumption that the wall deposits of vaseline aerosols build up a loose, dendritic structure which is permeable to the flow. In such a case additional amounts of particles would be removed by filtration. It is another consequence of this assumption that the deeper layers of the wall deposits should become less permeable in the course of time, and therefore a "saturation" in the amount of wall deposit should be observed for high loads. Such a trend is probably indicated in the graphs for stage 2 and stage 3. The wall deposits of stage 4 are substantially larger than those of stage 3 and stage 2, and in addition they scatter broadly between 1o % and 3o %, as indicated in fig. 3o. It is not clear if these high amounts are intrinsic to stage 4, or if they are related to the special mass size distribution which has a low and varying amount of mass in the size range of stage 4. From the observations one may conclude that the amount of wall deposit is higher when there are fewer particles above the size cut point of the stage.

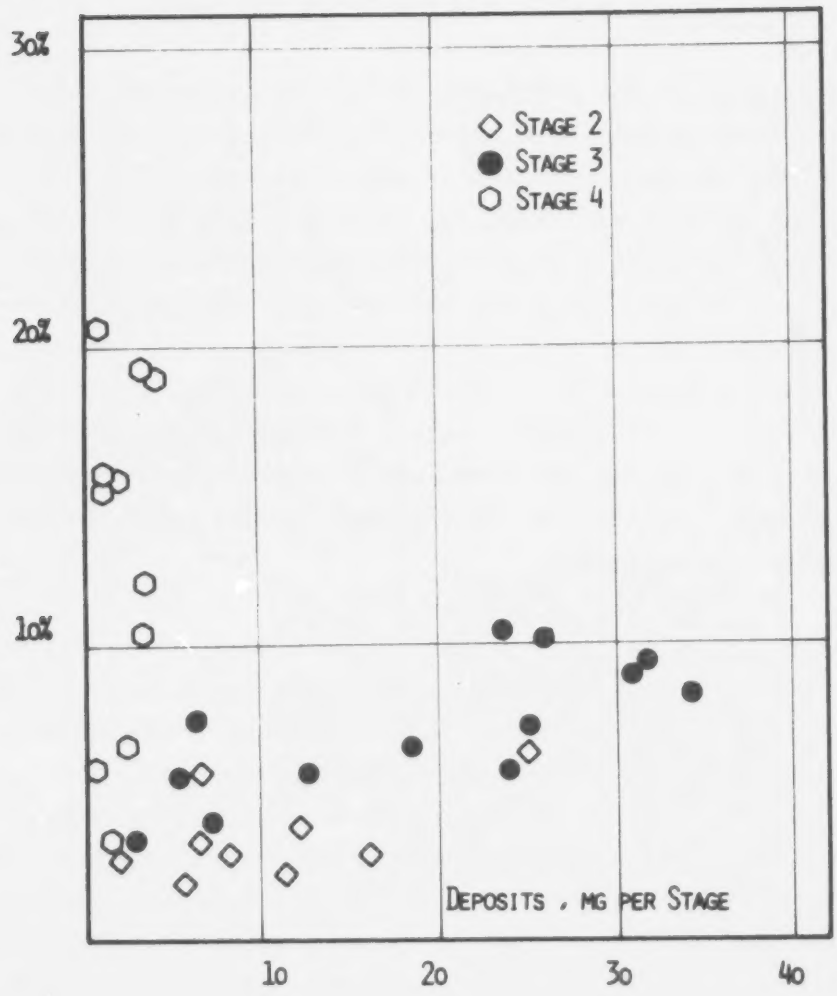

Fig.3o : Wall losses in the five stage impactor, with respect to a vaseline-dye-aerosol illustrated in fig.32.

The wall deposits of stage 1 have not been determined reliably enough for presentation of data at this time. However, the measurements indicate wall deposits in amounts of 1 % to 3 %.

Sample partitioning has been investigated by means of the vaseline-dye aerosol. After sampling the aerosol, the aluminum collection foils are cut into pieces, each one containing a spot. The mass is determined photometrically. The first results were discouraging, because deviations of 5 % to 1o % from the average spot mass occured (see fig. 31). However, these numbers were not in agreement with the flow measurements for single orifices, which indicated errors within 1 % to 2 % of the average flow. It turned out, that the discrepancy is related to the procedure of filling the aerosol chamber used in these experiments. If this chamber is filled inhomogeneously, the impactor collects on one side particle-free air for a longer period of time than on the other side. This has been proven twofold. First, homogenization of the chamber aerosol by stirring the air during filling lowers the deviations to acceptable limits of 2 % to 3 % of the average spot mass (see fig. 31). Secondly, at non-uniform filling the deviations exhibit systematic structures like maxima or minima, and these occur in the same angular positions with respect to coordinates of the chamber, irrespective of the angular position of the stages relative to the impactor (see fig. 31). Moreover, the results indicate that the flow in the impactor does not mix up even after having passed several stages.

In routine work the samples are weighed with a semi-micro balance with a reproducibility of $\pm$ 1o μg. The weight of blank aluminum foils is determinable with total errors of $\pm$ 15 μg to $\pm$ 2o μg depending on the skill of the experimenter and on the atmospheric conditions. The errors introduced by the routine sampling procedure are still higher. In this case the blank aluminum foils are transferred from the balance directly to the stages, and after closing and opening the impactor, are weighed again. By these manipulations, the errors increase to a total of $\pm$ 3o μg to $\pm$ 4o μg. (The manipulation errors would increase still more, if the foils were stored in containers). Such error limits are quite satisfactory for most practical purposes. The quality of the method is demonstrated by comparing the mass

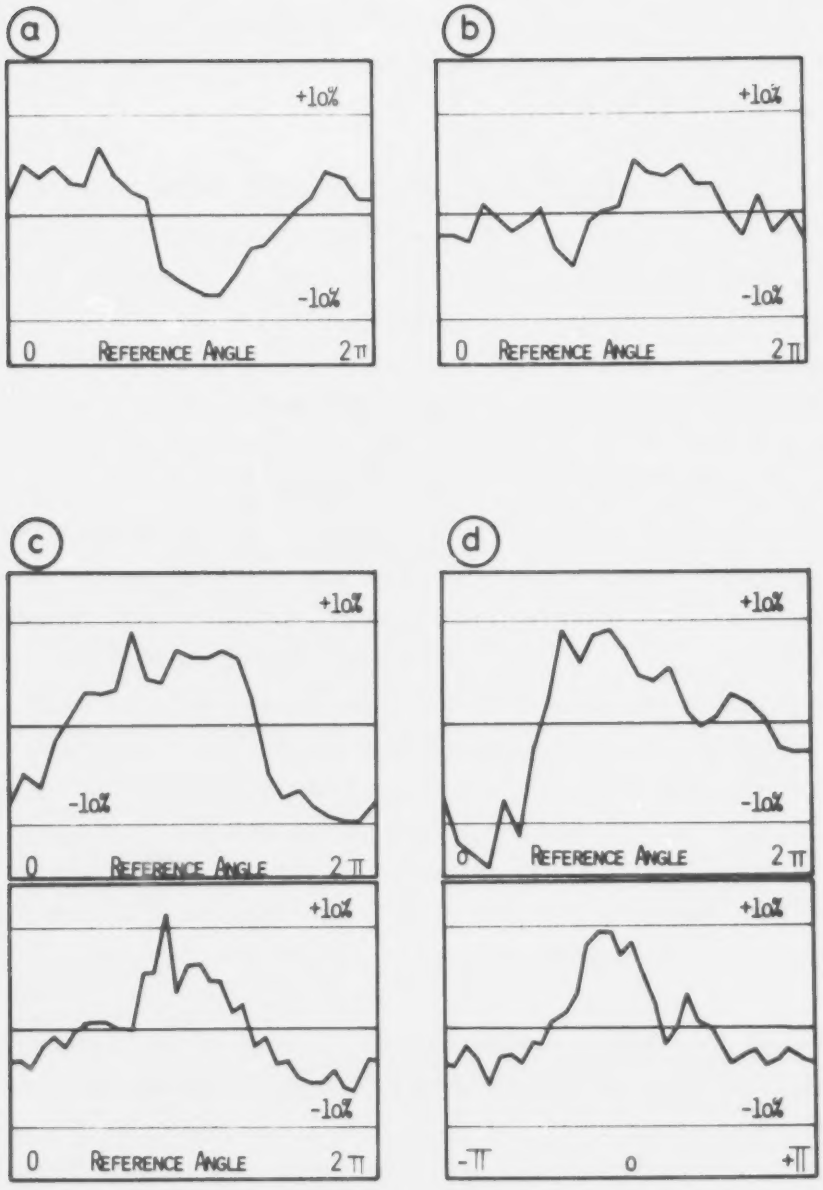

Fig.31: Variations of deposited mass among the spots of stages 2 and 3 of the impactor, at inhomogeneous (a) and homogeneous (b) sampling conditions. Examples (c) and (d) illustrate the mass variations for subsequent impactor stages.

FIG.32

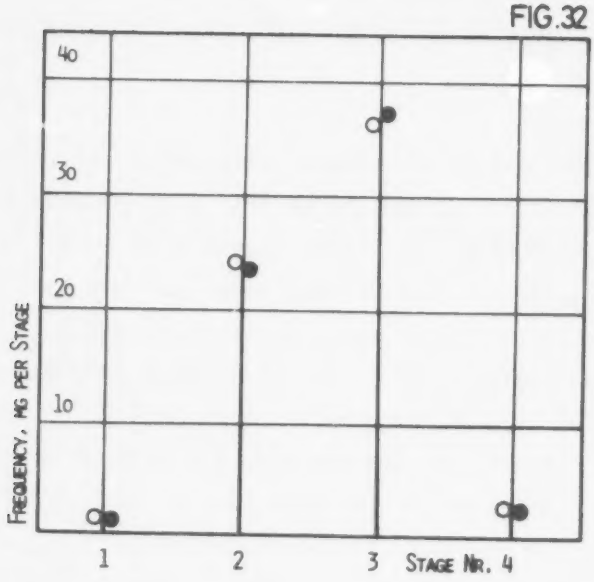

FIG.33

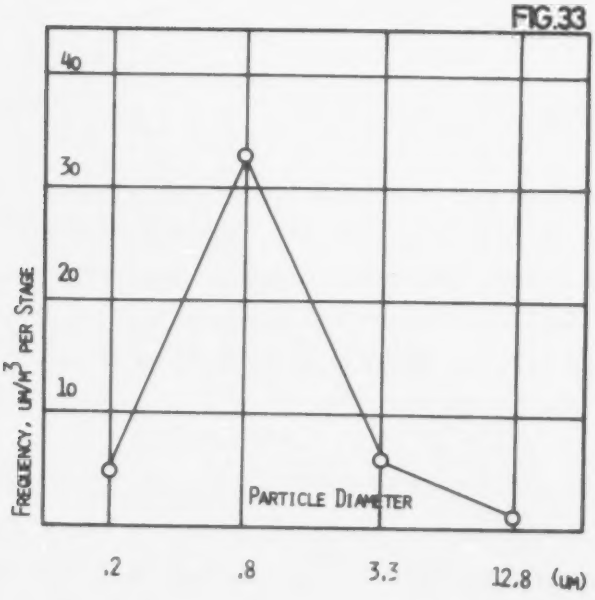

Fig.32: Mass size distribution of a vaseline-dye-aerosol by gravimetry (black dots) and photometry (open dots).

Fig.33: Mass size distribution of an urban aerosol at Vienna.

size distribution by gravimetry to the mass size distribution by photometry (see fig. 32).

First measurements of urban aerosol were performed in January 1978. The sampling station is on an open balcony 10 m above ground in the back yard of the institute building. Sampling periods of three to four hours proved to be sufficient for reliable measurements. The mass size distributions show definitely the accumulation mode of the urban aerosols (see fig. 33). The modal equivalent diameter is in the size range from 0,4 µm to 1,6 µm for all size distributions during the sampling period. Coarse particles are rare because of the height above ground and because of the remote position of the sampling site with respect to the dust sources. A series of subsequent measurements during several days has been conducted. These aerosols exhibit uniform mass size distributions with respect to shape, but the particle concentration vary strongly during the day, reflecting the variations of the strength of the sources as well as the variations of the atmospheric exchange conditions (see fig. 34).

Note on backup filters

Constant flow rates are necessary for operating impactors correctly. Consequently the pressure drop across the impactor, or the pressure in the final stage must be controlled. This is easily achieved by critical orifices at the exit of the impactor. According to our experience the method is practicable even for heavier deposits because these do not influence the flow resistance of the stages.

Backup filters will introduce additional resistances which have different initial values and are changing continuously due to the filter loading. These problems may be overcome by carefully selecting the filter material, or by automatic and manual control of the pressures. With respect to labour and equipment, however, these measures are more expensive than critical orifices.

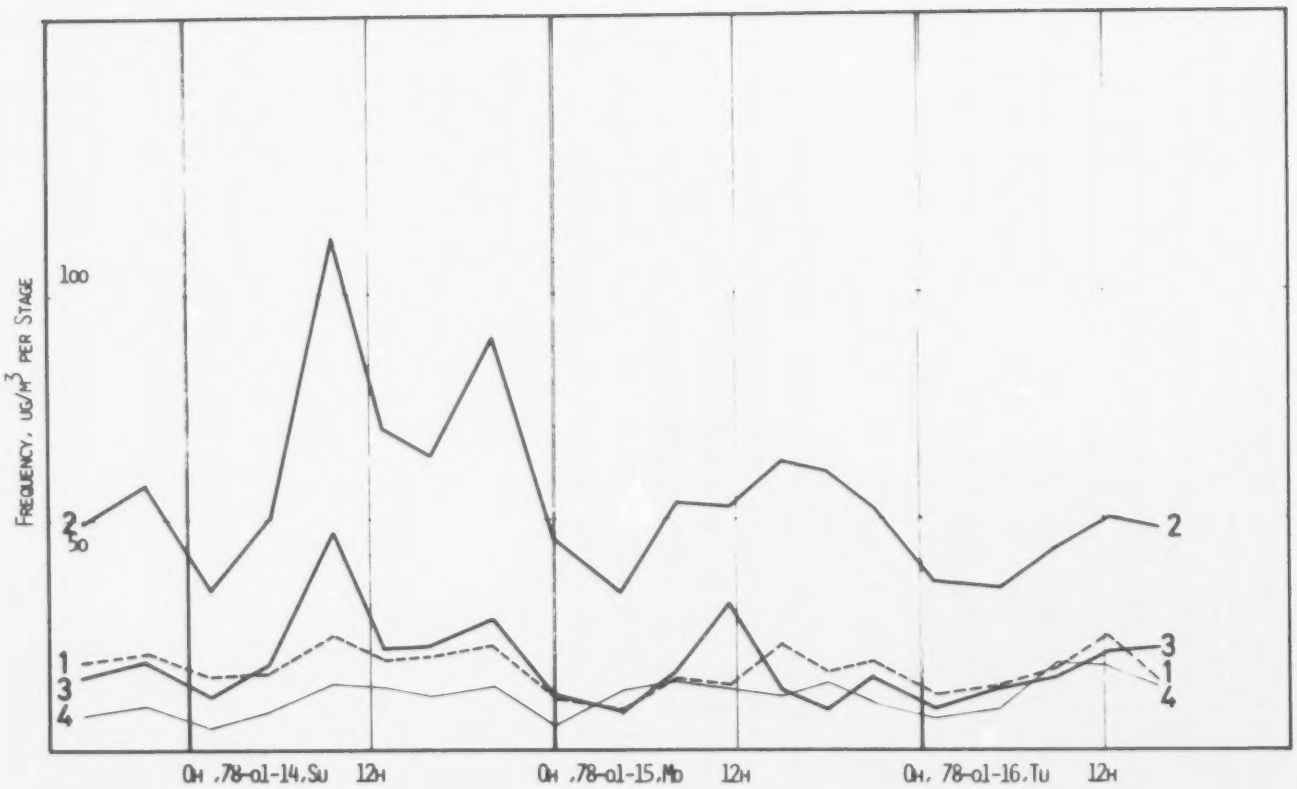

Fig. 34: Threehourly variations of urban aerosols at Vienna during a period of three days in february 1978. Numbers 1), 2), 3), 4) indicate the mass concentrations on stage 1),2), 3),4) of the impactor.

For a given aerosol the need of a backup filter depends on the properties of the impactor. The Viennese urban aerosols, e.g., exhibit an almost log normal mass size distribution in the fine particle range, with a mode in the range from o,5 µm to o,7 µm. The standard deviation is such that the size range below o,1 µm does not contribute considerably to the total mass of the aerosol. In this case the low pressure impactor with its final cut off size of o,1 µm will deliver a fairly valid estimate of the total aerosol mass; commonly used impactors, however, would not because their final stages have cut off sizes around o,5 µm or larger. These impactors are to be equipped with backup filters, or additional stages, in order to complete the data on the aerosol.

Nevertheless there might be interest in the ultrafine particles, especially when questions arise about their chemical nature. To meet such needs the low pressure impactor should be equipped with another stage, rather than with a backup filter. The stage would permit the application of critical orifices for flow control and it would offer the advantage of concentrating the particles on small areas, compared to the area of adequate backup filters.

THE CONDENSATION NUCLEI COUNTER

Introduction

Condensation Nuclei Counters (CNC's) are frequently used to measure the particle concentration in the atmosphere. However, it is not clear, if all atmospheric particles are activated as condensation nuclei, grow to visible size and can be detected. Investigations of the heterogeneous nucleation in supersaturated vapor are required to determine detection limit and sensitivity of CNC's. Furthermore, additional information about the nuclei aerosol can be obtained from measurements at different supersaturations.

The Expansion Cloud Chamber and its data acquisition system

Over a period of several years an expansion cloud chamber with digital process control and on-line data acquisition has been developed (5o). The experimental arrangement is shown in fig. 35. The necessary supersaturations are generated in a pressure-defined subpressure expansion cloud chamber EXP. For observation, the droplets, growing in the expansion cloud chamber, are illuminated by a He-Ne laser beam. During the expansion process and the subsequent droplet growth three parameters are monitored and recorded in the memory of a digital storage oscilloscope (transient recorder TR):

1) Gas pressure in the expansion chamber, measured by a piezoelectric pressure transducer PT.

2) Intensity of the light scattered by the growing droplets under a selectable fixed scattering angle, measured by the photomultiplier PM.

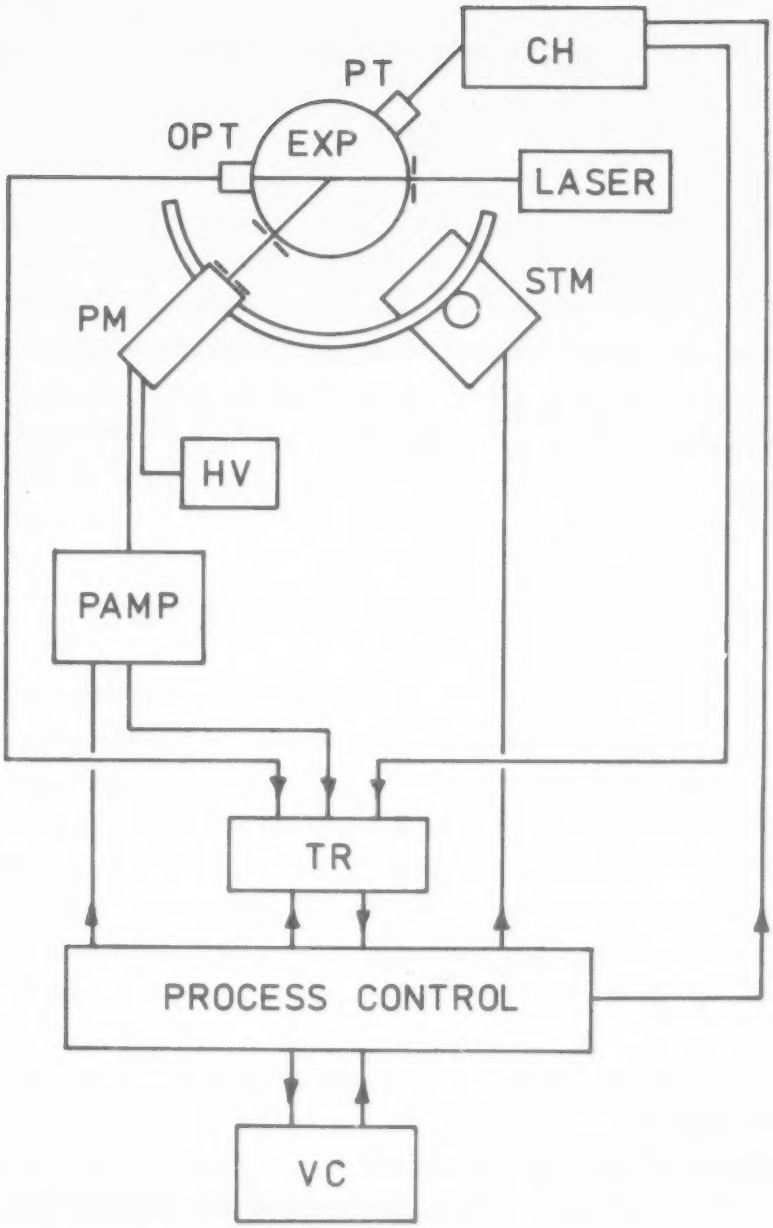

Fig.35: Diagram of the data acquisition system of the condensation nuclei counter.

3) Intensity of the light transmitted through the expansion chamber, measured by the opto-element OPT.

Because of the high data rate during a single measuring run it appeared to be necessary to interface the experimental apparatus to a digital computer (Digital Equipment Corp., PDP 15/3o). The data, obtained during each measuring run are stored on magnetic tape. Temperatures of the humidifier, the measuring chamber, and the ambient pressure are recorded continuously. According to a selectable measuring program different expansion ratios and scattering angles are chosen automatically. In case a malfunction is detected, the system is shut off after saving the already recorded experimental data.

The scattering intensity varies over more than two orders of magnitude, as the scattering angle is changed. Therefore it was necessary to develop a programmable amplifier PAMP for amplification of the light scattering signal. Depending on the actual intensity, adequate amplification is selected automatically.

Gas flow and pressure during each measuring run are controlled and maintained by two pumps and five solenoid valves. The valves are operated by an electronic valve control VC. The corresponding experimental arrangement is shown in fig. 36. Constant flow in the humidifier HUM is provided by the tubing pump TP in connection with V1 and the bypass valve V4. By means of the vacuum pump P in connection with the differential pressure transducer DP and valves V3 and V5 a preset subpressure is obtained in the recipient R1. The expansion is initiated by opening of valve V2. The measuring volume and the low pressure system are separated by a thin rubber membrane. The degree of supersaturation obtained is reproducible within a range of less than $\pm$ o,5 %. The expansion time is about 5 msec.

A typical set of experimental data from a single measuring run is shown in fig. 37. The upper curve shows the pressure as a function of time, the middle curve the transmitted light intensity and the lower curve the scattering

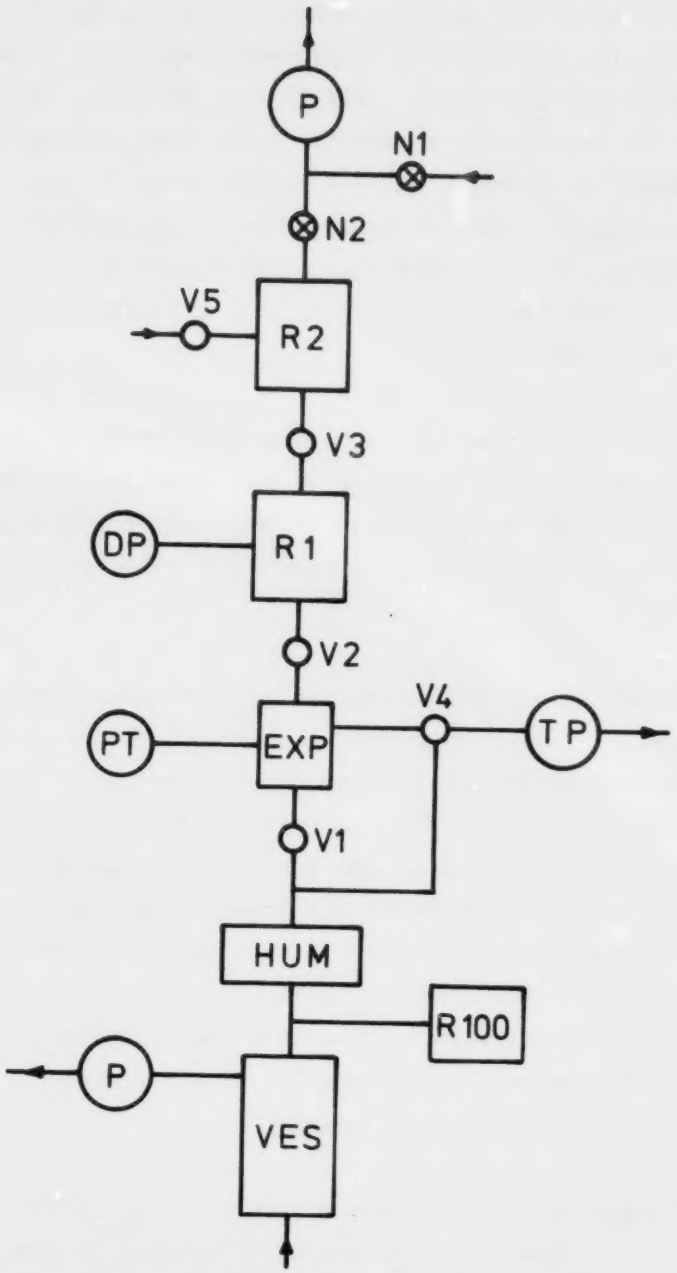

Fig.36: Aerosol and gas flow diagram of the condensation nuclei counter.

intensity. It can be seen that the expansion is completed before the growing droplets become visibile. Therefore, one can conclude that the influence of the growing droplets on the thermodynamic parameters in the measuring chamber is negligible during the expansion. Accordingly, vapor depletion and the release of latent heat of condensation will not change the initial supersaturation obtained and the expansion is dry-adiabatic.

The Analysis of the Recorded Data

The scattering intensity (fig. 37, lower curve), shows a series of maxima and minima (51). Fig. 38 shows theoretical light scattering curves for a single droplet. The good agreement between these curves indicates that the droplets are quite monodisperse. While for the experimental data the abscissa is a time axis, for the theoretical curves the abszissa is a size axis. Accordingly, after establishing a one-to-one correspondence between the extremes in the experimental and theoretical intensity curves, size and concentration of the droplets can be determined at various times during the growth process (52). From the position of the experimental extremes relative to the time axis the droplet size can be determined. On the other hand, the height of the experimental maxima is a quantitative measure for the droplet concentration. It should be stressed that this procedure provides an absolute method for independent measurement of droplet size and concentration. At high droplet concentrations the light extinction in the measuring chamber cannot be disregarded. Therefore the measured height of the experimental light scattering maxima must be corrected. Dividing the light scattering signal by the light intensity, transmitted through the expansion chamber, will eliminate the extinction effect.

It turned out that the experimental droplet growth curves are very sensitive to temperature changes in the expansion chamber and the humidifier. Therefore a two stage thermostating system was used which reduced temperature variations to $\pm$ 0,005 K. For an accurate determination of the initial supersaturation in the measuring chamber a precise knowledge of the expansion ratio is essential. Measurement of the gas pressure using the piezoelectric pressure transducer (PT, fig. 35) with a response time as small as 5 µsec

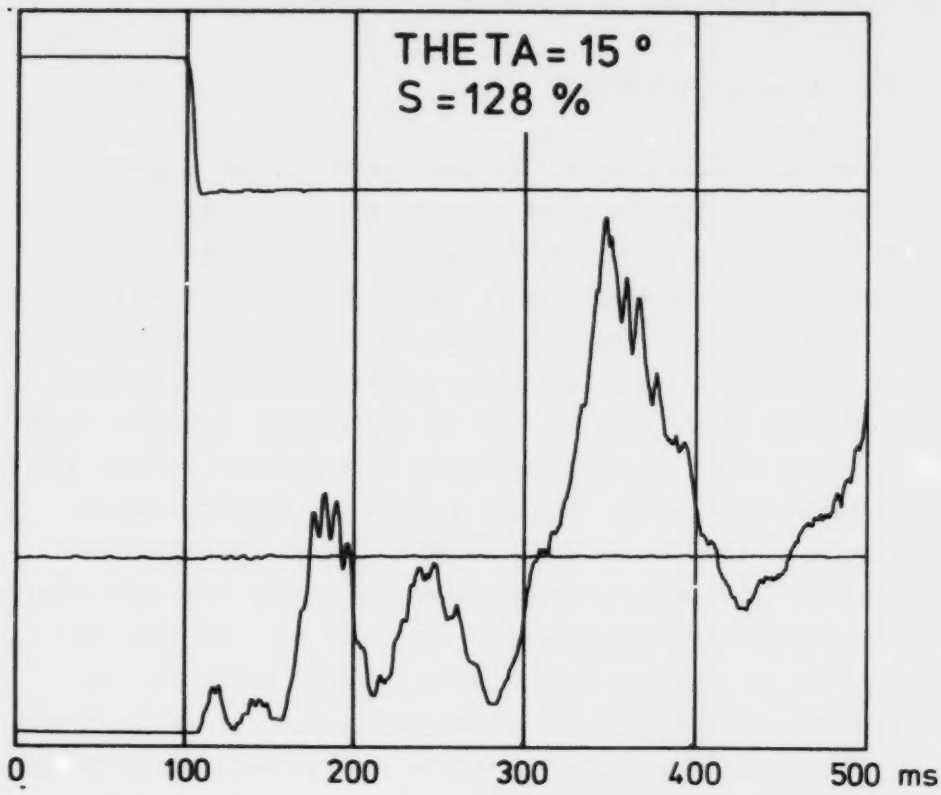

Fig.37: Scattered light intensity of the growing aerosol, recorded at a scattering angle of 15^{o} .

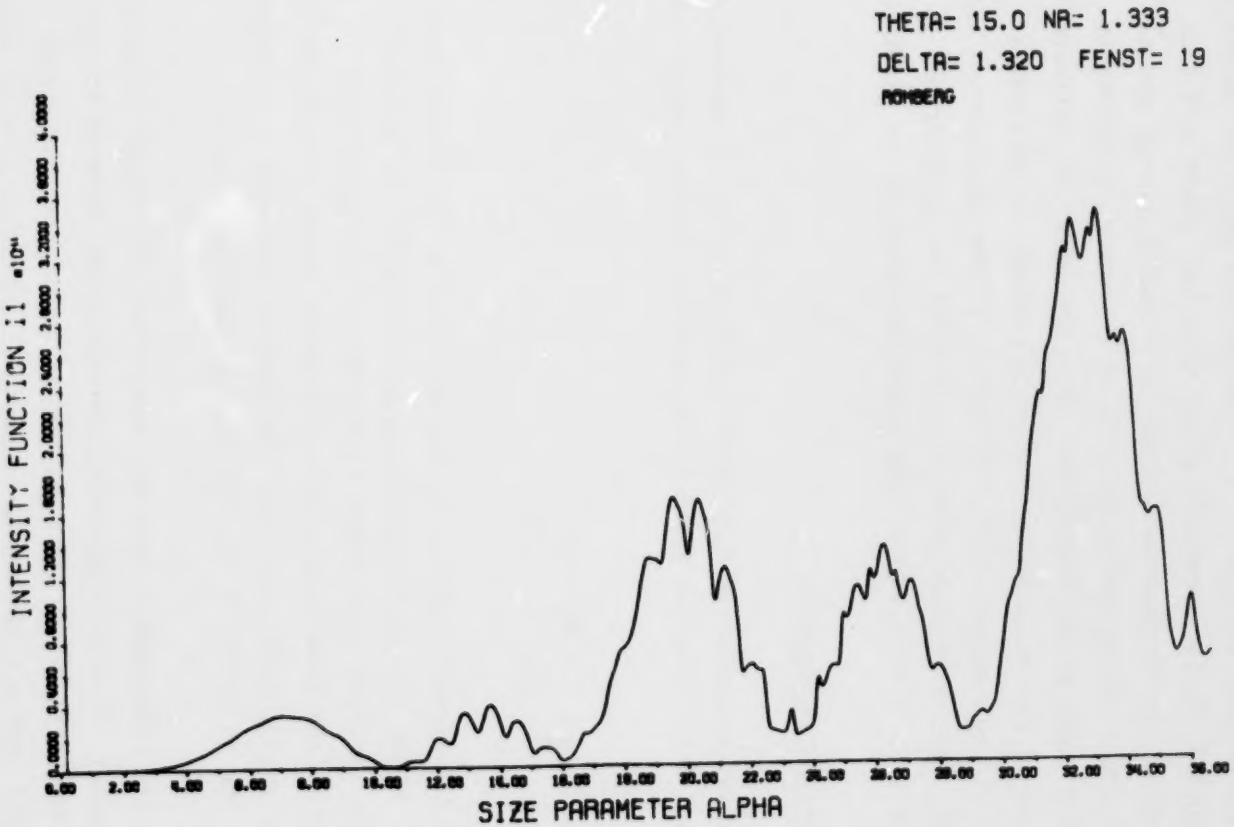

Fig.38: Scattered light intensity calculated from the MIE theory for a scattering angle of 15^{0} .

allows a determination of the supersaturation with an error of less than ±.5 %.

Measurements of droplet concentration have been performed at different supersaturations between 1o3 and 4oo %. Urban aerosol particles served as condensation nuclei. At low supersaturations only the larger particles will start to grow. As the supersaturation is increased during several measuring runs, more and more particles will be activated. According to the Gibbs-Kelvin equation the lower size limits for particles activated at given degrees of supersaturation, can be calculated. In this way a cumulative "Kelvin-equivalent"-size distribution of the condensation nuclei can be obtained. This equivalent size of a particle can be described as the size of a water drop growing at the same supersaturation as the particle.

Results on Atmospheric Aerosols

Fig. 39 shows a cumulative size distribution which can be derived from the experimental data using the Kelvin-Gibbs-equation for the equivalent diameter

$$d = \frac{4.\sigma.M_V}{R.\rho_L.T} \cdot \frac{1}{\ln S}$$

Here σ denotes the surface tension, M_V the molecular weight of the vapor, ρ_L the density of the liquid, S the supersaturation and T the absolute temperature. The particle sizes range from 0,002 to 0,11 µm diameter. Differentiation of the cumulative size distribution yields a differential particle number distribution (Fig. 4o). The mode of this size distribution corresponds to the so called Nucleation Mode of the urban aerosol.

The indicated experimental data are mean values over about 1o measuring runs for each point. To obtain statistically significant data on the urban aerosol, long measuring series are required. It is expected that these measurements will give a clearer understanding of the urban aerosol in the range below 0,1 µm.

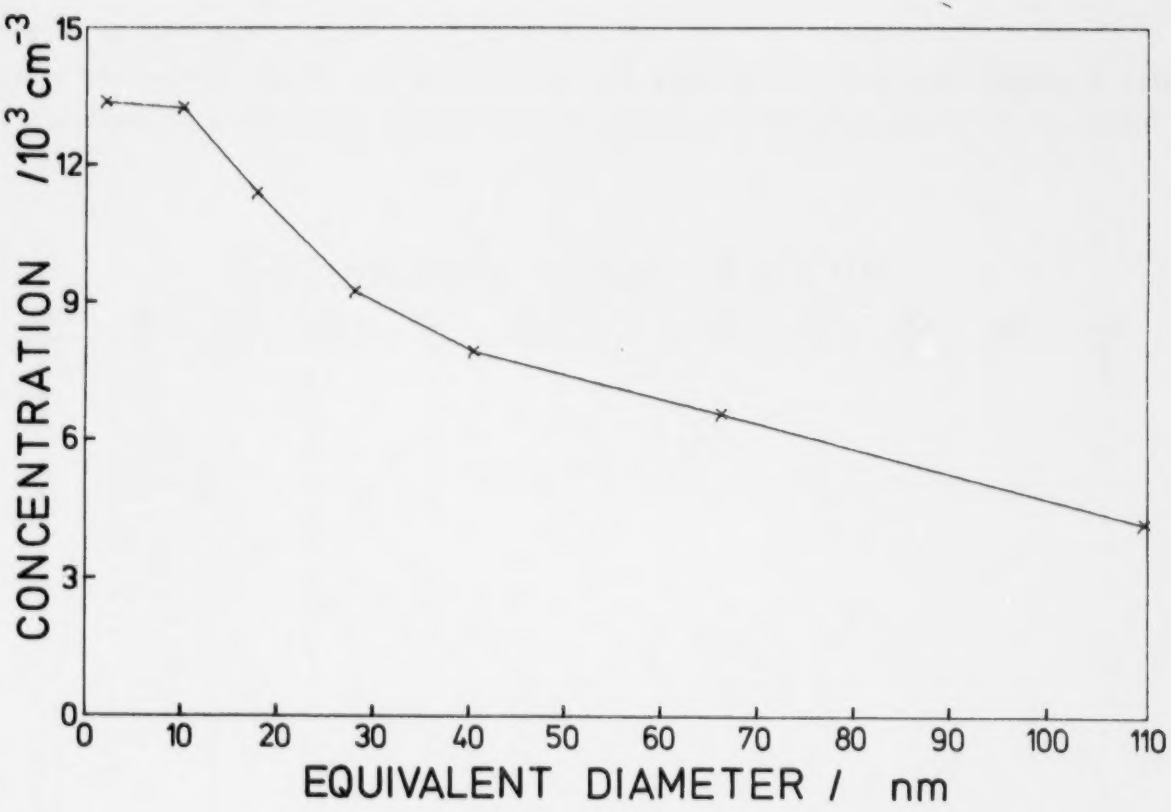

Fig.39: Cumulative number size distribution of KELVIN equivalent diameter for an urban atmospheric aerosol at Vienna.

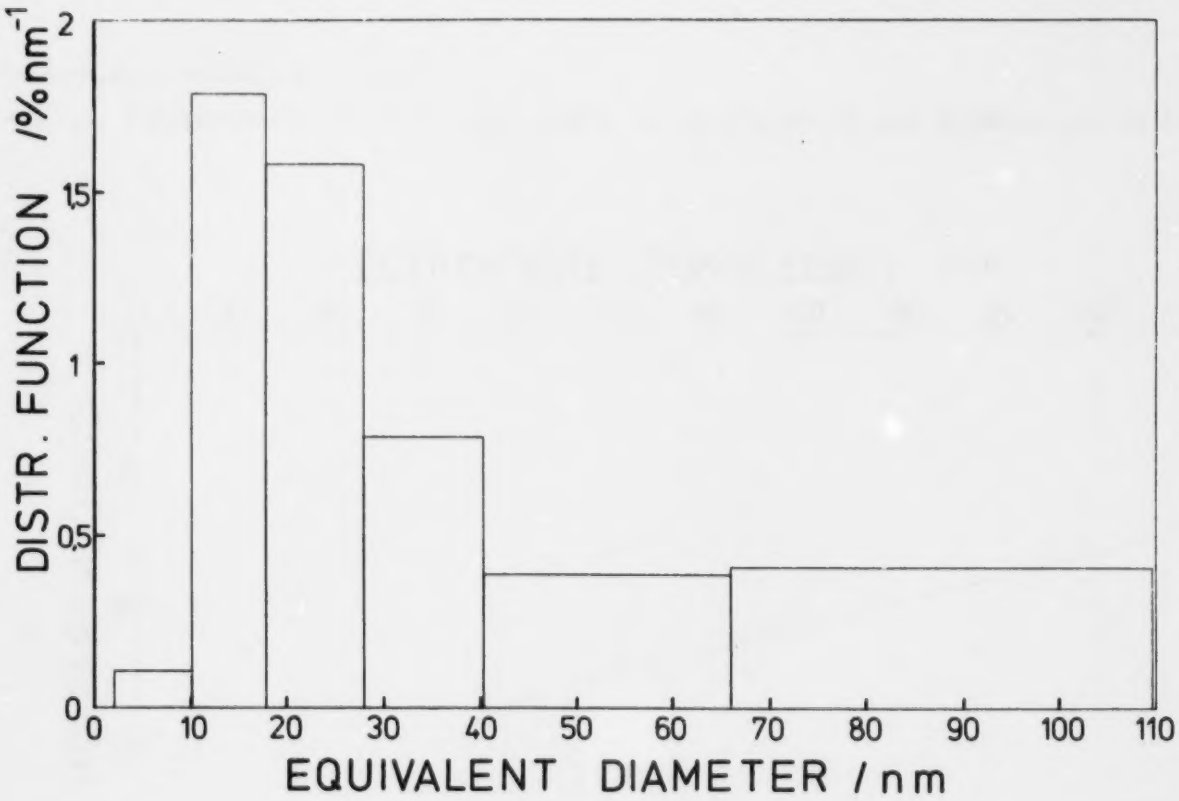

Fig.4o: Differential number size distribution of KELVIN eqivalent diameter for an urban atmospheric aerosol at Vienna. The distribution has been derived from the cumulative size distribution of fig. 39.

REFERENCES

1. Sawyer, K.F., and Walton, W.H. The Conifuge - A size-separating sampling device for airborne particles, J. Sci. Instruments 27 (195o), p. 272

2. Goetz, A. An Instrument for the quantitative separation and size-classification of airborne particulate matter down to o.2 micron. Geofisica Pura e Appl. Proc. II, 36, (1957), p. 49

3. Goetz, A. Stevenson, H.J.R. and Preining, O. The Design and Performance of the Aerosol Spectrometer. A.P.C.A. Journal 1o (196o) p. 378

4. Goetz, A. and Preining, O. Bestimmung der Größenverteilung eines Aerosols mittels des Goetz'schen Aerosolspektrometers. Acta Physica Austriaca, 14 (1961) p. 292

5. Keith, C.H. and Derrick, J.C. Measurement of the particle size distribution and concentration of cigarette smoke by the "conifuge". J. Coll. Science, 15 (196o), p. 34o

6. Kast, W. Neues Staubmeßgerät zur Schnellbestimmung der Staubkonzentration und der Kornverteilung. Staub, 21 (1961), p. 215

7. Stöber, W. and Zessak U. Zur Theorie einer konischen Aerosolzentrifuge. Staub, 24 (1964), p.295

8. Stöber, W. und Zessak U. Zur Messung von Aerosol-Teilchengrößenspektren mit Hilfe von Zentrifugalabscheidern. Zentralblatt für Biologische Aerosolforschung, 13 (1966), p. 1

9. Stöber, W. and Flachsbart, H. Aerosol Size Spectrometry with a Ring Slit Conifuge. Environmental Sci., 3 (1969) p. 641

1o. Stöber, W. and Flachsbart, H. High Resolution Aerodynamic Size Spectrometry of Quasi-Monodisperse Latex Spheres with a Spiral Centrifuge. J. Aerosol Sci., 2 (1971), p. 1o3

11. Stöber, W., Flachsbart, H. and Boose, Ch. Distribution Analyses of the Aerodynamic Size and the Mass of Aerosol Particles by Means of the Spiral Centrifuge in Comparison to other Aerosol Precipitators. J. Coll. Sci. 39 (1972), p. 1o9

12. Stöber, W., Design and Performance of a Size-Separating Aerosol Centrifuge Facilitating Size Spectrometry in the Submicron Range. In: Assessment of Airborne Radioactivity. Vienna, International Atomic Energy Agency, 1967.

13. Hauck, J. und Schedling, J.A. Ober ein modifiziertes Modell einer Konifuge. Staub 29 (1969), p. 18

14. Hochrainer, D. and Brown, P.M. Sizing of Aerosol Particles by Centrifugation. Environmental Sci. and Technology, 3 (1969), p. 83o

15. Hochrainer, D. A New Centrifuge to Measure the Aerodynamic Diameter of Aerosol Particles in the Submicron Range. J. Coll. Interface Sci., 36 (1971), p. 191

16. Berner, A. und Reichelt, H. Ober Einlaßspaltsysteme in Konifugen. Teil I: Das ROSL-System. Staub 29, (1969), p. 92

17. Burson, J.H., Keng, E.Y.H., and Orr, C.,Jr. Particle Dynamics in Centrifugal Fields. Powder Technology 1 (1967) p. 3o5

18. Matteson, M.J., Boscoe, G.F. and Preining, O. Design Theory and Calibration of a Field Type Aerosol Spectrometer. Aerosol Sci. 5 (1974), p. 71

19. Abed-Navandi, M., Zum Auflösungsvermögen des Aerosolspektrometers, Ph.D. Dissertation, Vienna 1973

2o. Abed-Navandi, M., Berner, A. and Preining, O. The Cylindrical Aerosol Centrifuge in:Fine Particles, B.Y.H. Liu Ed., Academic Press, London, New York, 1976

21. Stöber, W., Berner, A. and Blaschke, R. The Aerodynamic Diameter of Aggregates of Uniform Spheres. J. Coll. Int. Sci. 29 (1969), p. 71o

22. Stöber, W. and Boose, Ch. Developing Flow and Particle Deposition in Horizontal Elutriators and Semi-Dispersive Aerosol Centrifuges. Atmospheric Env. 7 (1973) p. 119

23. Townsend, J.S. The Diffusion of Ions into Gases. Proc. Roy. Soc. 65 (19oo) p. 192

24. Gormley, P.G. and Kennedy, M. Proc. Roy. Irish Acad. 52 A (1949), p.163

25. Tan, C.W. Diffusion of Disintegration Products of Inert Gases in Cylindrical Tubes. Int. J. Heat Mass Transfer 12 (1969), p. 471

26. Tan, C.W. and Hsu, C.J. Diffusion of Aerosols in Laminar Flow in a Cylindrical Tube. J. Aer. Sci. 2 (1971), p. 117

27. Sinclair, D. A Portable Diffusion Battery. Its Application to Measuring Aerosol Size Characteristics. Amer. Ind. Hyg. Ass. J. 33 (1972), p. 729

28. Matteson. M.J., Sandlin, C.W. and Preining, O. Diffusion of Aerosols at Various Temperatures. J. Aer. Sci. 4 (1973) p. 3o7

29. Kasper, G. Untersuchungen der Durchlässigkeit einer kompakten Diffusionsbatterie im Temperaturbereich von + 35°C bis -75°C. Ph.D. Dissertation, Vienna, 1977.

3o. Kasper, G., Preining, O. Penetration of a Multistage Diffusion Battery at Various Temperatures. J. Aerosol Sci. 9 (1978) p. 331

31. Kasper, G., Berner, A. Ein Generator zur Erzeugung extrem monodisperser Kochsalzaerosole. Staub-Reinh. Luft 38 (1978) p. 183

32. Matteson, M.J., Fox, J.J. and Preining, O. Density Distribution of Sodium Chloride Aerosols Formed by Condensation. Nature Phys. Sci. 238 (1972) p. 61

33. Kasper, G. On the Density of Sodium Chloride Aerosols Formed by Condensation. J. Coll. Interface Sci. 62 (1977), p. 359

34. Espenscheid, W.F., Matijevic, E. and Kerker, M. Aerosol Studies by Light Scattering: III. Preparation and Particles Size Analysis of Sodium Chloride Aerosols of Narrow Size Distribution. J. Phys. Chem. 68,(1964),p.2831

35. Armbruster, L., Stahlhofen, W. und Gebhart, J. Produktion von monodispersen Feststoffaerosolen nach dem La Mer-Sinclair-Prinzip. in: Tagungsbericht Ges. f. Aerosolforschung, Bad Soden/BRD, 1976.

36. Kasper, G. Membrane Filter Mounts and a Quick-change Device for Aerosols and Liquid Suspensions. J. Physics E: Sci. Instr. 1o, (1977), p. 6oo

37. Holländer, W. and Schumann, G. On the Influence of Image Forces on the Performance of Diffusion Batteries. in: Tagungsbericht Ges. f. Aerosolforschung, Bad Soden/BRD, 1976.

38. Davies, C.N. Diffusion and Sedimentation of Aerosol Particles from Poisseuille Flow in Pipes. J. Aer. Sci. 4 (1973), p. 317

39. Taulbee, D.B. and Yu, C.P. Simultaneous Diffusion and Sedimentation of Aerosols in Channel Flows. J. Aer. Sci. 6 (1975), p. 433

4o. Thomas, J.W.
Particle Loss in Sampling Conduits
in: Assessment of Airborne Radioactivity,International Atomic Energy Agency, Vienna, 1967.

41. Towney, S. Bull. Observ. Puy de Dome 173 (1963).

42. Pich, J. Impaction of Aerosol Particles in the Neighborhood of a Circular Hole. Coll. Czech. Chem. Commun. 29 (1964).

43. Smith, T.N. and Phillips, C.R. Inertial Collection of Aerosol Particles at Circular Aperture. Env. Sci. Techn. 9 (1975), p. 564.

44. Spurny, K. Zentralbl. biol. Aerosolforschung, 13 (1966), p. 44

45. Smutek, M. and Pich, J. Impaction of Particles on the Surface of Membrane Filters. J. Aer. Sci. 5 (1974), p. 17

46. Spurny, K. and Pich, J. Staub 24 (1964), p. 25o

47. Spurny, K. and Madelaine, G. Czech. Chem. Commun. 29 (1971), p. 2857

48, Berner, A. Zur Abscheideeigenschaft von Impaktorstufen bei nicht stationärer Strömung. Sitzungsber. Österr. Akademie der Wissenschaften, Mathem.-Naturw. Klasse Abt. II, 185. Bd. (1976), p. 327

49. Berner, A. Zur Ursache sekundärer Partikelniederschläge bei Impaktoren Staub-Reinh. Luft 38 (1978), p. 1

5o. Wagner, P.E. und Pohl, F.G., Eine prozeßgesteuerte Anlage zur Untersuchung der Kinetik von Kondensationsvorgängen. Staub-Reinh. Luft 38 (1978),p.72

51. Wagner, P.E. Optical Determination of the Size of Fast-growing Water Droplets in an Expansion Cloud Chamber. J.Coll.Interf.Sci.44 (1973),p.181

52. Wagner, P.E. The Interdependence of Droplet Growth and Concentration. I. Theory of Droplet Growth and Applications on Condensation Nuclei Counters. J. Colloid Interface Sci. 53 (1975), p. 429

53. Porstendörfer, J., Heyder, J. Size Distributions of Latex Particles. J. Aerosol Sci. 3 (1972), p. 141

54. Heard, M.J., Wells, A.C., Wiffen, R.D. A Re-determination of the Diameters of DOW Polystyrene Latex Spheres. Atm. Environm. 4 (197o),p.149